Stony Brook University

Electrical Methods to Characterize Defect Evolution in Plasma Sprayed Coatings under Cyclic Straining

A Thesis Presented

by

Arash Ghabchi

to

The Graduate School

in Partial Fulfillment of the

Requirements

for the Degree of

Master of Science

in

Materials Science and Engineering

Stony Brook University

December 2007

Stony Brook University

The Graduate School

Arash Ghabchi

We, the thesis committee for the above candidate for the Master of Science

degree, hereby recommend

acceptance of this thesis.

Dr. Andrew Gouldstone – Thesis Advisor

Assistant professor, Materials Science and Engineering

Dr. Richard Gambino

Professor, Materials science and Engineering

Dr. Jon Longtin

Professor, Mechanical Engineering

Stony Brook University

This thesis is accepted by the Graduate School

Lawrence Martin
Dean of the Graduate School

Abstract of the Thesis

Electrical Methods to Characterize Defect Evolution in Plasma Sprayed Coatings under Cyclic Straining

by

Arash Ghabchi

Master of Science

in

Materials Science and Engineering

Stony Brook University

2007

The focus of this research is to understand the microstructural changes that occur under low strain cycling of air plasma sprayed (APS) coatings. Preliminary data shows that under nominally elastic loading (<< 0.1% strain) of thermally sprayed materials changes occur that are detectable via electrical (resistivity, dielectric constant) measurement methods. This is due to the micro-scale growth of pre-existing defects. To systematically test this, we deposited spinel coatings on tapered cantilever substrates, which were flexed to provide spatially constant in-plane cyclic strains. After different numbers of cycles, dielectric constant of coatings was measured via impedance spectroscopy. Results confirm growth of defects under these low strains, and also a large effect of humidity on different porosity features. We explain this by recourse to physisorption and chemisorptions of water on crack faces. To understand the adsorption phenomena electrical measurements conducted on ceramic TS coatings. Our investigation could have major implications for coating reliability, as it allows us to characterize how a coating evolves in-service.

TABLE OF CONTENTS

LIST OF FIGURES

Chapter 1: Mechanics

1.1. Fatigue and failure of metals and ceramics

In the metallurgy, polymer science and mechanical engineering communities, the word *fatigue* is a well accepted term for describing the deformation and failure of materials under cyclic loading conditions. The expression *cyclic fatigue* is used in the ceramic community to describe cyclic deformation and fracture, and to differentiate it from static fatigue which is time-dependent failure driven by environmental interactions. [1]

Based on classification of the degree of brittleness by Lawn and Wilshaw, 1975, in non-brittle or ductile materials, such a, FCC metals, polymers and some BCC metals, dislocation movement (plasticity) plays a dominant role in cyclic deformation and fracture in the bulk and in the immediate vicinity of the crack tip as well. On the other hand in highly brittle materials, the controlling parameter in cyclic deformation and fracture is bond rupture which means strength of atomic bonds determines the fracture resistance of material. Thus, flaws play an important role in response of ceramics to cyclic load. Lawn and Wilshaw noted flaws in highly brittle solids are characterize by three features (1) the flaws need not to be large in size to affect the strength significantly, (2) the flaws are induced mainly on the surface of the material and also be introduced during processing, (3) the flaws exhibit wide variations in size, location and orientation.[2]

The characteristics of cyclic fatigue in ceramics are different from metals:

I. Fatigue cracks in ceramics do not initiate naturally; crack initiation is associated with some pre-existing defects.

II. Fractography of ceramic fatigue shows nominally identical fracture surface under monotonic and cyclic loads, and also the more debris and surface damages on the fatigue surfaces(C.J. Gilbert)

III. Microstructure has a significant effect on crack growth rate in ceramics.[5] Different authors have shown ceramics with different grain size exhibit various crack growth rate. ([4], Gilbert and Ritchie, 1997)

There are two possible classes of fatigue mechanism in ceramics:

I. *Intrinsic or crack tip mechanism:*
This mechanism happens at the tip of the crack and occurs under cyclic loads. In this mechanism crack advances by damage processes at the crack-tip region.

II. *Extrinsic or wake mechanism:*
This mechanism is applicable for ceramics that develop crack bridging. In this mechanism cyclic load degrades the strength of bridging ligaments.

Cyclic fatigue process in metals obeys intrinsic mechanism naturally, but the cyclic fatigue process in ceramics is extrinsic. Many authors [6-10] have considered that degradation of the crack bridges is because of the frictional wear of sliding ligaments when the crack opens and closes again and again under cyclic fatigue test.

If the effect of surface roughness in cyclic fatigue test is removed, by making smooth-surfaced specimens what is observed is a remarkable scattering in number of cycles-to-failure results which arises from flaw

population. These pre-existing defects (flaws) usually come from processing step and/or from sample preparation steps. In addition to above mechanisms, test environment can affect the fatigue life of material.

The simultaneous action of cyclic stress and chemical attack is known as corrosion fatigue [13]. For metals corrosive attack occurs at the surface of metal and produces pitting, this pitting can act as notches and reduce the fatigue strength of material. When corrosive and fatigue occur simultaneously, the chemical reaction accelerates the fatigue crack propagation. Bottoms of the pits are more anodic than the rest of the metal so that corrosion proceeds inward, aided by the disruption of the oxide by cyclic strain. For example, results of fatigue test for copper showing higher fatigue strength in the vacuum than air. water vapor acts as a catalyst to reduce the fatigue strength in air [14].

The mechanism proposed for *slow crack growth* in alumina single crystal is a stress-corrosion mechanism by water molecules [11]. G. de With *et. al* showed that fracture toughness decreases with increasing humidity for dense ceramics, that indicates adsorption of water plays important role in fracture. Similar behavior was seen in MnZn ferrites [12].

Importantly, in the case of introducing artificial cracks to the material, cyclic fatigue test results will be sensitive to initial flaw size.

1.2. Effective parameters on fatigue and failure of metallic and ceramic coatings

Coatings deposited on different substrates with different methods are being used in various industries such as aerospace, automotive, medical,

petrochemical, petroleum, pulp and paper industries. Coating reliability, lifetime and failure are dependent on the mechanical, physical and chemical properties, and also the operating environment. Fatigue plays an important role. Several examples of coating where initiation and progression of fatigue are critical, are shown below.

To overcome some mechanical, chemical and environmental issues in coating industries, High Velocity Oxy-Fuel deposition has been applied to deposit WC-Co with almost same hardness, wear and corrosion resistance, and a low coefficient of friction as electro plated chromium. With inducing a compressive stress field on the substrate, the nucleation and propagation of fatigue cracks can be arrested or delayed. The compressive stress field can be achieved by shot peening of the substrate [20-22].

1.2.1. Examples of different coating systems: Thermal Barrier Coatings

Thermal barrier coatings systems have been subjected to wide studies for understanding their durability which is governed by a sequence of crack nucleation, propagation and coalescence events that accumulate prior to final failure by large scale buckling and spalling.

1.2.1.1. Failure mechanism in Thermal Barrier Coating

The specific ways which the cracks nucleate and grow is related to increasing the severity of the imperfections (size of the imperfections) and thickness of thermally grown oxide (TGO) layer as the system is exposed and cycled. All causes an increasing in magnitude and scale of tensile stress.

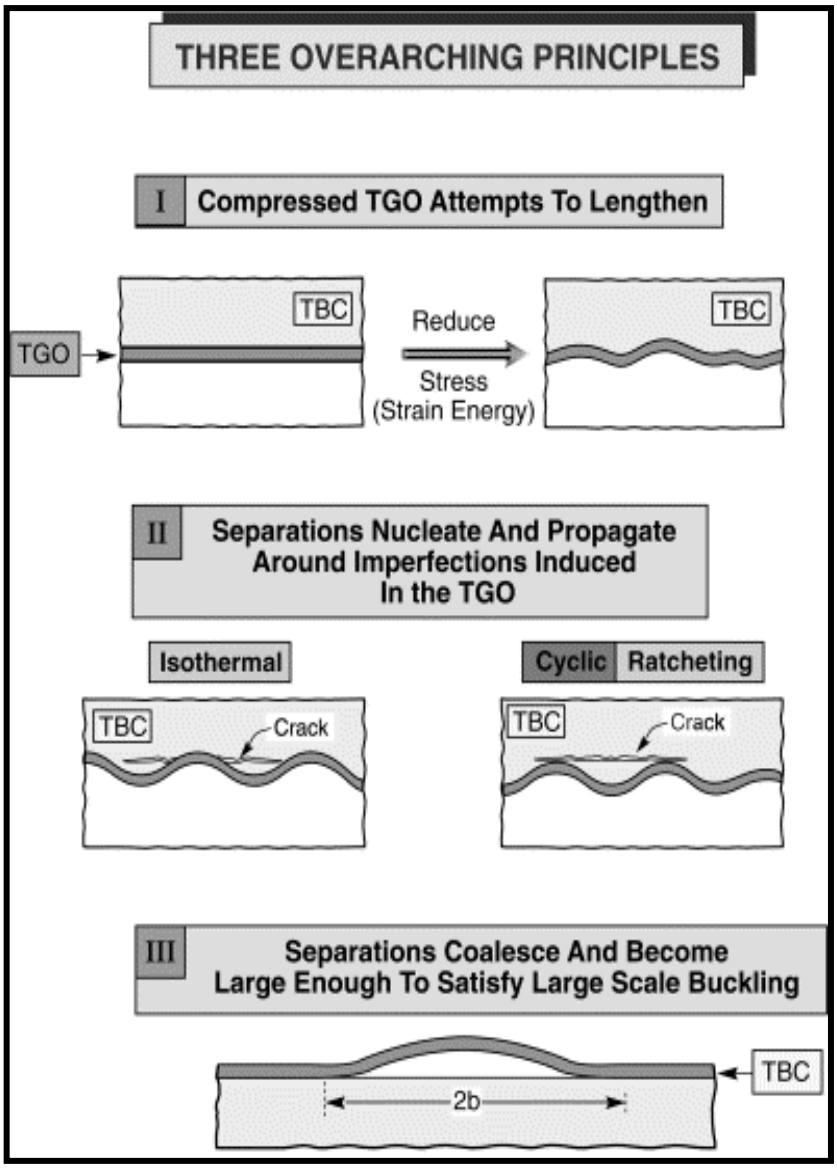

Figure 1 Sketch illustrating the overarching principles governing TBC failure [24].

Following that, the stresses act on cracks that nucleate and propagate around the imperfections [23]. Figure 1 shows three overarching principles govern the failure of TBC systems [24].

1.2.2. Biomedical implant coatings [25-27]

Biomedical coatings have been used on different implants within the body such as hip joints, knee joints, bone plates, etc to satisfy specific requirements such as a high degree of crystallinity for positive biological responses, good coating adhesion, optimal porosity and fatigue resistance Figure 2. However, surgical implants undergo degradation after 10 to 15 years of use. A biomedical implant can fail for different reasons. The following is the summary of common failures:

I. Deficiencies in design (size and shape) of the device for a particular patient (e.g., an undersized noncemented stem)

II. problems (e.g., problematic orientation or problems in wound healing)

III. Host abnormalities or diseases (e.g., osteopenia)

IV. Infection

V. *Material fracture, wear, and corrosion.*

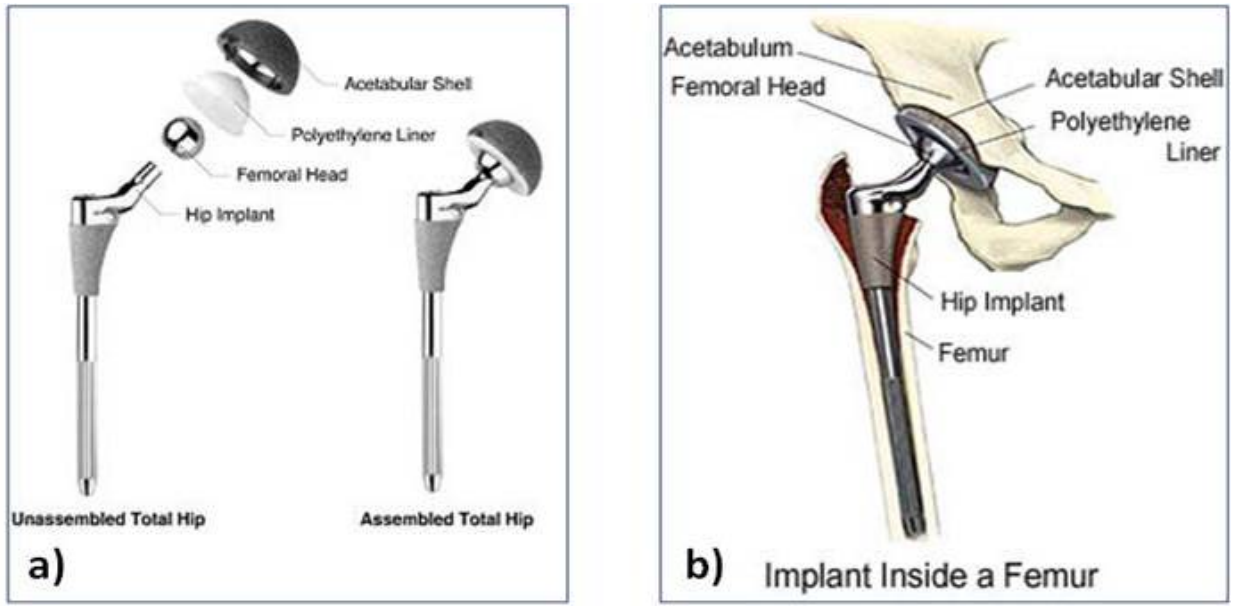

Figure 2. Total hip implant, a) unassembled and assembled, b) implant inside a femur[internet]

1.2.2.1. Failure mechanism of biomedical implants

1.2.2.2. Fracture and wear

For load-bearing implants, fracture happens in both implant and bone. Figure3. Fracture eventually leads to failure of implant. From environmental point of view, bio-environments are mostly wet. In wet atmosphere sliding wear resistance compared with dry atmosphere is lower. Other mechanisms for increased in vivo wear include environmental stress cracking, polymer degradation, microstructural imperfections, and creep. This wear may cause poor mechanical fir between the ball and socket of the hip.

1.2.2.3. Corrosion and corrosive fatigue

Sub-surface fatigue is the second type of wear. High contact stresses in the artificial joints will cause a crack in the biological materials that will propagate beneath the surface.

Corrosive fatigue is due to cyclic loading and corrosive biological environment (human body). The fracture in this system is due to three main factors:

I. Porosity at the grain boundaries
II. Intergranular corrosive attack
III. Cyclic fatigue loading

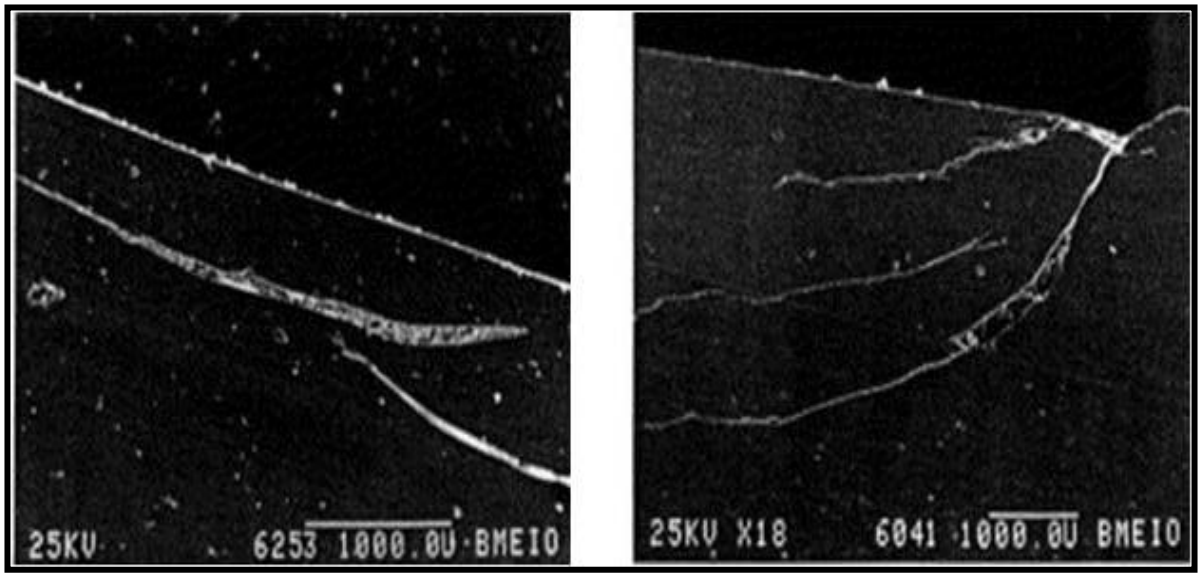

Figure 3. A typical knee crack[28]

1.2.3. Hydroxyapatite coating for implants

Due to hyroxyapatite(HA) advantages in vivo behavior, it is one of the successful implant coating materials. Air plasma spray (APS) method has been used to produce HA coatings on Titanium substrates. Due to difference between thermal expansion coefficient of coating and substrate, near the interface of plasma sprayed coating and substrate, coating is experiencing residual stresses. In general, residual stress increases with increasing thickness of coating and temperature of plasma spraying. This residual stress can have effect on fatigue strength and bonding strength of the coating. In this case having surface roughness for growing bone tissue into the coating material is decisive, but with increasing the roughness, fatigue life will be decreased. Obtaining optimal amount of surface roughness is crucial. Fatigue life of biomedical implant coating is crucial because even one small part of coating falls off, replacement surgery will be necessary and it is similar to implant failure.

1.2.4. Layered and compositionally graded films

Diffusion of atomic species during the processing or work period of thin films (time, temperature) and multilayer films causes local variation in composition and microstructure. Such variation can affect the stress evolution, damage and cracking behavior of overall coating (Suresh and Mortensen 1998). Compositional gradient can also be produced purposely to enhance the mechanical performance of coating by controlling stress, inelastic deformation or damage at specific sites such as surfaces, corners and interfaces. Examples include carburizing and nitriding processes (treatments). This compositional gradient can be achieved by means of different deposition methods such as

physical vapor deposition (PVD), chemical vapor deposition (CVD), thermal spray, sintering, three-dimensional printing and combustion synthesis.

At critical crack nucleation sites such as interfaces and sharp corners where interfaces between dissimilar materials intersect free surfaces, thermal and residual stresses can remarkably reduce by introduction of continuous or step-wise compositional gradient [29].

Considering above coating systems, it is decisive to keep in mind following effective parameters for fatigue and failure of various coatings:

I. Residual stress state presents in the coating (compression or tension) that originates from processing step. Existence of tensile stress in the coating reduces the fatigue life of coating and substrate as well.
II. Magnitude of that residual stress in the coating. Higher the residual tensile stress, lower the fatigue life of the component. This is better to calculate the average residual stress based on residual stress profile of the coating. (Residual stress varies from the top of the coating toward the substrate.)
III. Surface roughness of coating. The fatigue crack initiation is known as a surface phenomenon which is also related to the residual stress level near the surface. Rough surface provides stress concentrated spots and yielding of material happens locally in that high stressed region (crack initiation stage) and that crack propagates.
IV. Presence of pre-existing flaws, defects and cracks within the material and their size. Material containing pre-existing has more stress concentration sites and those cracks can propagate easier under cyclic fatigue load (smaller crack initiation stage).

V. Environmental condition and exposure time can cause erosion, corrosion, or gas phase embrittlement, which all affect fatigue life. As mentioned in previous chapter humidity can have effect on fatigue life of brittle ceramics, especially for those that adsorb more amounts of hydroxy ions.

Chapter 2: Impedance Spectroscopy

Impedance Spectroscopy (IS) is a very versatile tool to characterize intrinsic electrical properties of any material and its interface. The basis of IS is the analysis of the impedance (resistance of alternating current) of the observed system in subject to the applied frequency and exciting signal. This analysis provides quantitative information about the conductance, the capacitance (dielectric constant), the static properties of the interfaces of a system, and its dynamic change due to adsorption or charge-transfer-phenomena. IS uses alternating current with low amplitude. This facilitates a non-invasive method for detailed observation of structural-functional studies of many systems without any or less influence on the electrical and chemical state. These systems can be metallic, ceramic and liquid. This is especially so of systems in which important processes occur at the molecular level, such as processes associated with biological and synthetic memranes and interfaces that form between solutions and various solids. Four-terminal digital spectrometer provides resoulution about 0.002% in impedance magnitude and 0.01° in phase in a frequency range of 10^{-2} to 10^{5} Hz.

2.1. Fundamentals [30]

Impedance measurement is made by applying small alternating current (a.c.) with known frequemcy ω and small amplitude i_o to the system and measuring the amplitude v_o and phase difference ϕ of the concomitant electrical potential that develops across it. Impedance is given by

Equation 1 $$|z| = \frac{v_0}{i_0}$$

In Cartesian coordinates, impedance becomes a complex number

Equation 2 $$Z = R + jX \text{ where } j = \sqrt{-1}$$

The real and imaginary parts of Z describe the resistance (R) and reactance (X) and can be represented by appropriate electrical circuit elements in series.

2.1.1. The impedance of a homogeneous system

The impedance of a homogeneous material may be expressed in terms of a conductance elemnt G in parallel with a capacitance element C. Figure 4

Equation 3 $$Z(\omega) = \frac{1}{G + j\omega C}$$

Parameter G describes ability of homogeneous material to conduct and parameter C describes the ability of homogenous material to store electrical charge. For a slab of cross sectional area A and thickness x, these properties are given by

Equation 4 $$G = \sigma\frac{A}{x} \text{ and } C = \varepsilon\frac{A}{x}$$

Where the constants σ and ε are the electrical conductivity and dielectric permittivity of material.

2.1.2. Impedance of heterogeneous system

A heterogeneous system can be defined by number of different homogenous material (slabs) are sandwiched together. The total impedance will be

Equation 5 $$Z_o = \sum_{n=1}^{N} \frac{1}{G_n + j\omega C_n}$$

2.1.3. Dispersions of conductance and capacitance

In a simple multilayered system as mentioned above it is convenient to describe and present the impedance in terms of the overall parallel conductance G(ω) and capacitance C(ω) at a particular frequency.

Equation 6 $$Z(\omega) = \frac{1}{G(\omega) + j\omega C(\omega)}$$

For a single slab (N=1), the overall parallel conductance and capacitance will be

Equation 7 $$G(\omega) = G_1 \; and \; C(\omega) = C_1$$

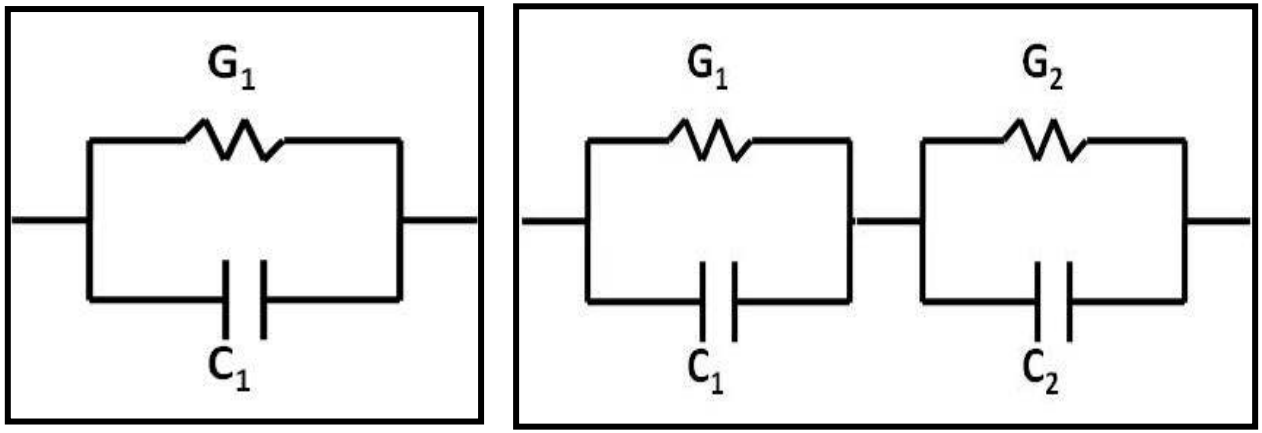

Figure 4 Equivalent circuits for a single-layer and two-layer system.

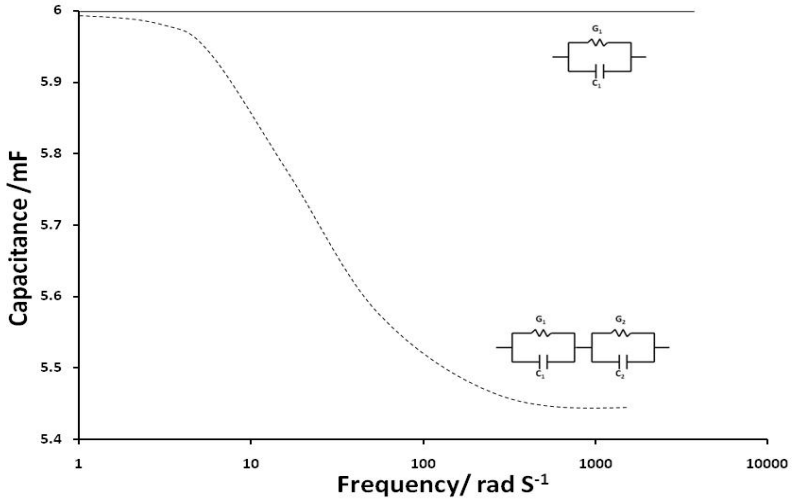

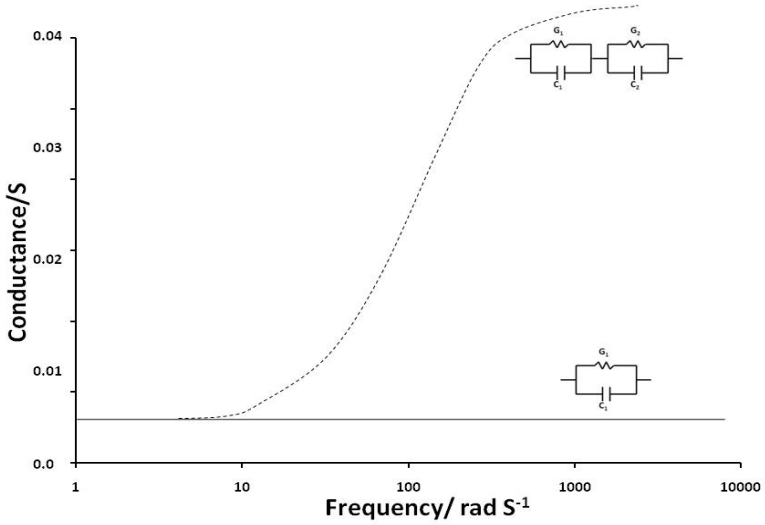

Figure 5 Conductive and capacitive properties for single layer and double-layer system [30]

As we see in this equation conduction and capacitive properties are constant at a particular frequency. But for multilayer system (N>2) these two properties disperse with frequency Figure5. The shape of the dispersion curve depends on the number of layers (N) [30].

2.1.4. Interfacial polarization

Interfacial polarization occurs whenever there is an accumulation of charge at an interface between two materials or between two regions within the material. The simplest example is interfacial polarization due to accumulation of charges in the dielectric near one of the electrodes, as shown in Figure6. Even a perfect material contains defects and impurities. In Figure6.a) the material has an equal number of positive ions and negative ions, but in this case, positive ions are considered to be mobile. This assumption is based on size of positive ions (smaller than ions) in ceramics. Under the applied electrode filed these positive ions will migrate toward the negative electrode and pile-up near the electrode and give rise to a positive space charge near the electrode. This additional charge on the electrode appears as an increase in dielectric constant.

Another mechanism for interfacial polarization is accumulation of electrons or holes at defects at the crystal surface, at the interface between the crystal and the electrode. In the presence of electric field, positive charges move to the negative electrode and get trapped in defects at the interfaces. Grain boundaries and interfaces in heterogeneous dielectric materials lead to interfacial polarization. Figure6.c

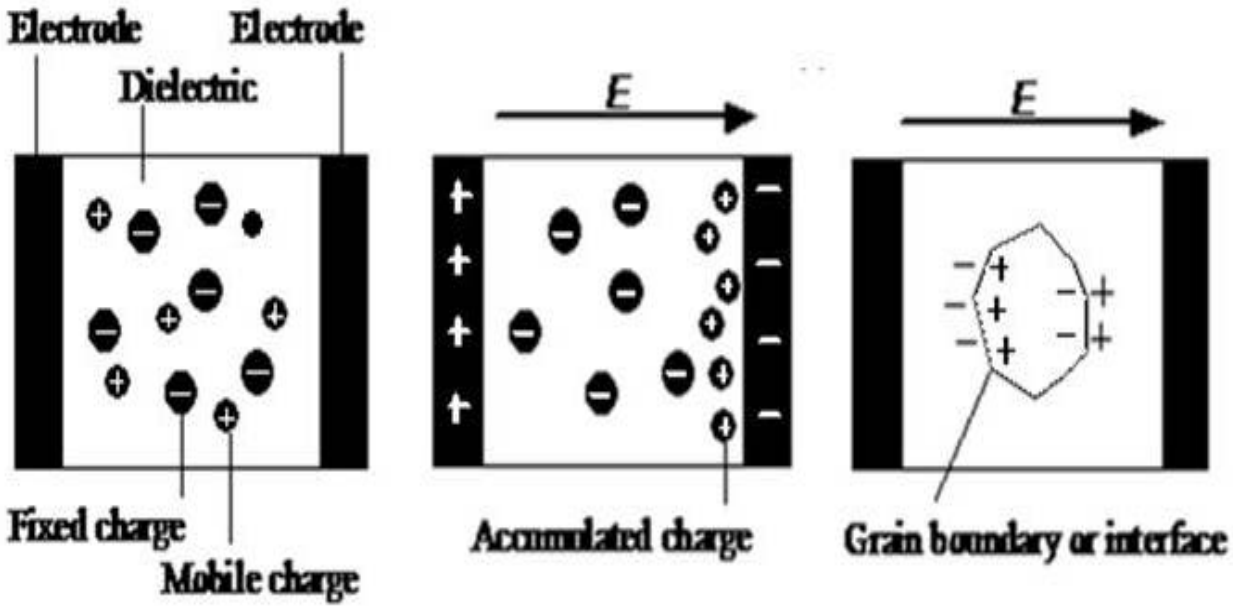

Figure 6. a crystal with equal number of positive mobile ions and negative fixed ions(a) in the presence of applied field positive ions migrate toward the negative electrode ad accumulate there(b) grain boundaries and interfaces give rise to interfacial polarization [31].

Dielectric constant: Frequency and temperature dependent

2.1.4.1. Frequency dependent

The static dielectric constant is an effect of polarization under dc conditions. When the applied field to a parallel plate capacitor is a sinusoidal signal, then the polarization of the medium under this ac condition leads to an ac dielectric constant. We generally write the complex dielectric constant as

Equation 8 $$\varepsilon_r = \varepsilon_r' - j\varepsilon_r''$$

Where ε_r' is the real part and ε_r'' is the imaginary part and both of them are frequency dependent as shown in Figure7. The real part represents the relative permittivity that we would use in calculating the capacitance. The imaginary part represents the energy lost in the dielectric medium as the dipoles are oriented against random collision one way and the other way and so on.

Figure 8, presents the features of frequency dependence of the real and imaginary parts of the dielectric constant. In reality the peaks of imaginary part and other features of real part are broader. There is no one particular lattice vibration frequency. Moreover, the polarization effects depend on the crystal orientation. In the case of polycrystalline materials, different materials in different directions overlap to exhibit a broadened overall peak. At lower frequencies the interfacial polarization features are even broader because there can be a number of conduction mechanisms for the charge to accumulate at interfaces, each having its own speed.

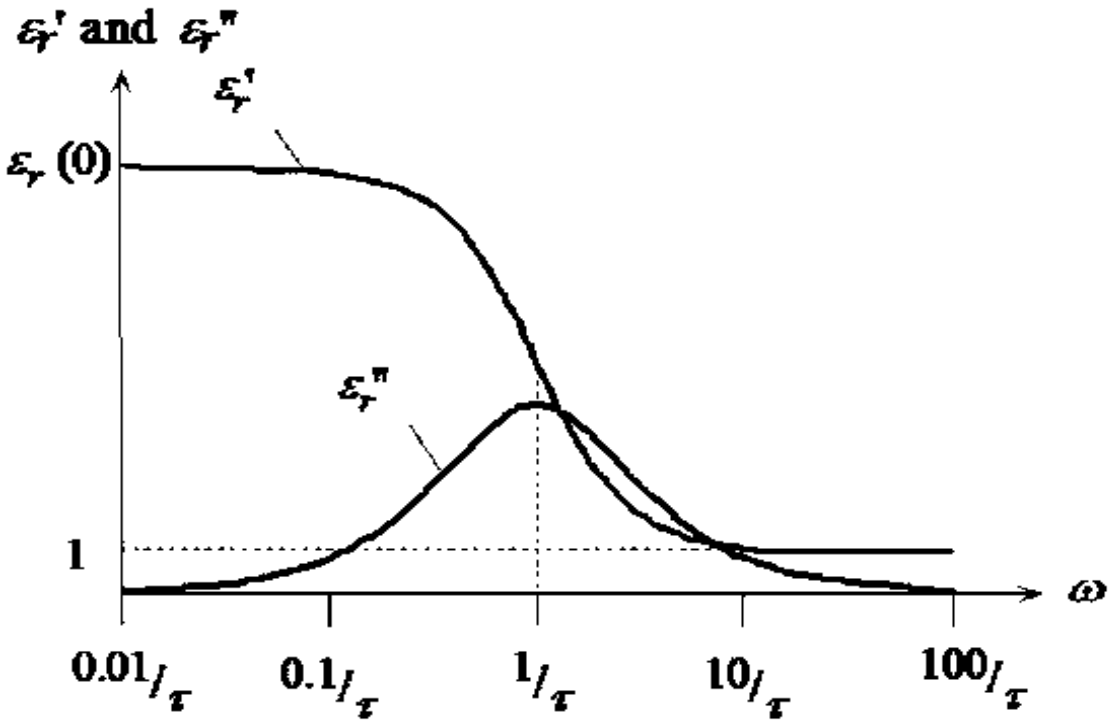

Figure7. the real and imaginary part of ac dielectric constant, exhibits relaxation at $\omega = 1/\tau$ [31].

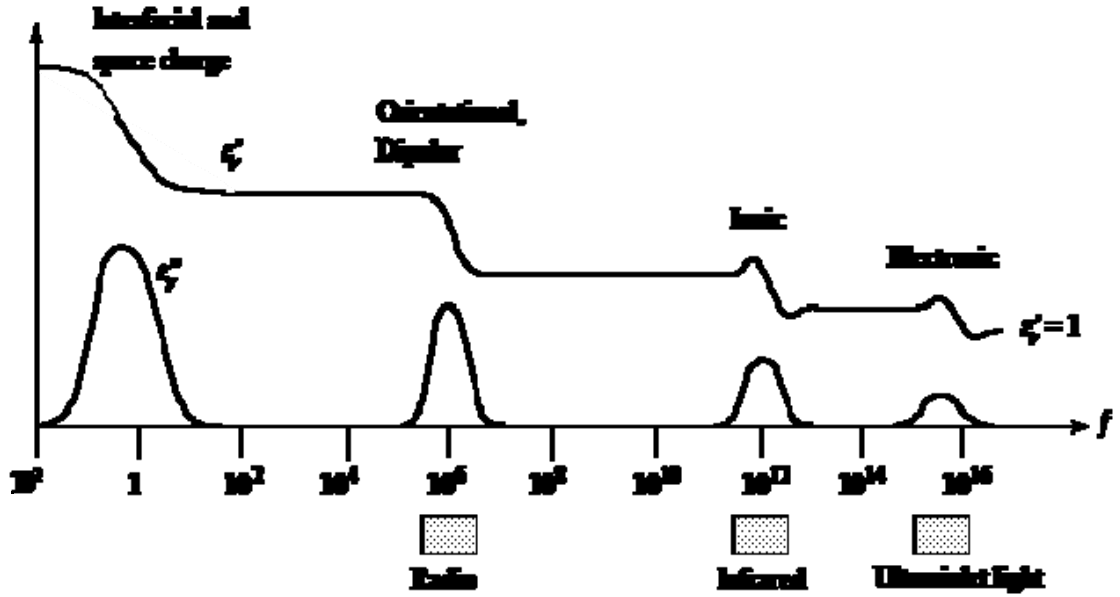

Figure 8. frequency dependence of imaginary and real parts of dielectric constant in the presence of interfacial, orientational, ionic and electronic polarization [31].

2.1.4.2. Temperature dependence of dielectric constant

The capacitance C of a parallel plate capacitor is

Equation 9 $$C = \varepsilon\varepsilon_0 \frac{A}{d}$$

Where ε_0 is permittivity of free space, A is the area and d is the distance between two parallel electrodes. Differentiation of above equation gives

Equation 10 $$TCC = \frac{1}{C}\left(\frac{\partial C}{\partial T}\right)_p = \frac{1}{\varepsilon}\left(\frac{\delta\varepsilon}{\partial T}\right)_p + \alpha$$

Where α is the linear expansion coefficient, and from

Equation 11 $$\frac{1}{\varepsilon}\left(\frac{\partial\varepsilon}{\partial T}\right)_p = \frac{(\varepsilon-1)(\varepsilon+2)}{\varepsilon}(a+b+c)$$

$(a = -\alpha)$ then for most insulators,

Equation 12 $$TCC = \frac{(\varepsilon-1)(\varepsilon+2)}{\varepsilon}(-\alpha+b+c) + 0.05tan\delta + \alpha$$

Above equation can be radically implified for given ranges of ε, as shown in Figure 9. When tanδ = 0.1% extrinsic, CTE becomes dominant [51].

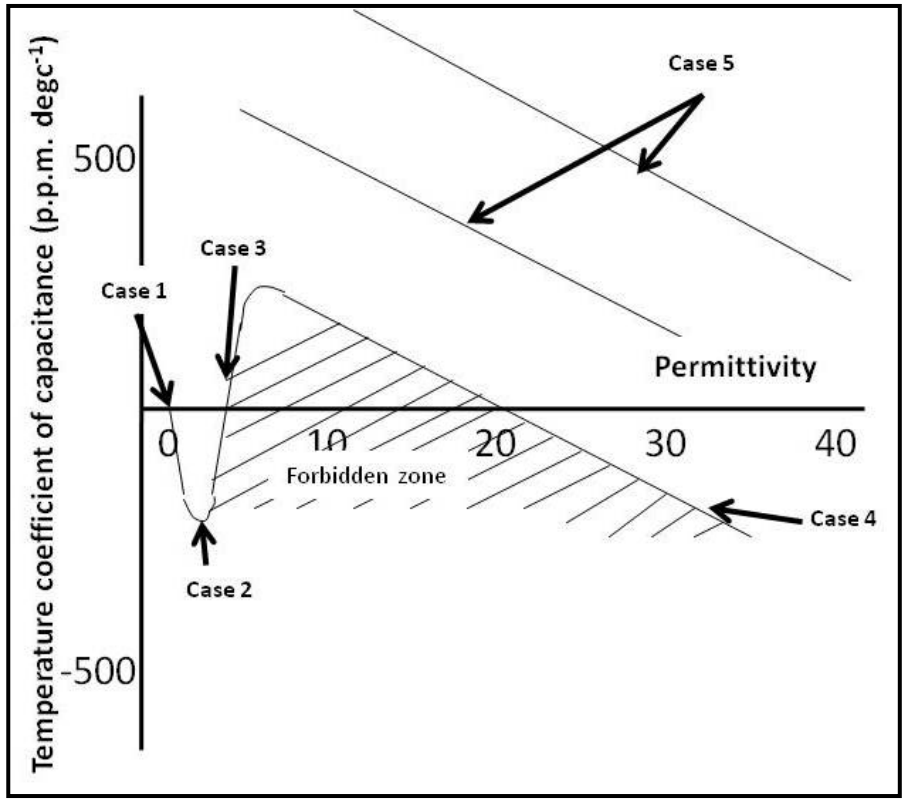

Figure 9. Temperature coefficient of capacitance plotted against permittivity, lines correspond to the cases with different losses and ε. [51].

Different cases are

Case 1. $\varepsilon = 1$

This is a vacuum, TCC = 0.

Case 2. $1.5 < \varepsilon < 2.5, tan\delta < 0.1\%$

$TCC \approx -\alpha$

Case 3. $2.5 \leq \varepsilon \leq 10$

In this case TCC is not well-defined. In the middle of this region the TCC passes from a negative value (electronic polarizability) to a positive value (ionic polarizability).

Case 4. $\varepsilon \geq 10, tan\delta \leq 0.1\%$

$TCC \approx G - \alpha\varepsilon$

Case 5. $\varepsilon \geq 10, tan\delta > 0.1\%$

$TCC = 0.05 tan\delta - \alpha\varepsilon$

This gives a series of straight line for different losses, as shown in figure.

2.2. Application of impedance spectroscopy in evaluation of coatings' durability

Recently impedance spectroscopy received extensive interest as non-destructive method for evaluation of various coatings. This method has been successfully applied to thermally sprayed coatings, particularly TBCs, to evaluate failure, high-temperature oxidation, degradation, and nucleation and growth of cracks and defects (damage detection) of TBCs. As mentioned before, failure of TBCs initiates in the reaction layer due to thermal mismatch stress with a non-planar interface. It has been reported that $Ni(Cr,Al)_2O_4$ (spinel structure) and NiO formed above 1000°C during the oxidation of TBC systems. It was suggested that these two oxides were detrimental to durability of TBCs due to the rapid local volume increase [32-36]. W.R. Chen *et.al* studied role of certain oxides in causing crack nucleation and growth. They found out that crack initiated mostly in association with the formation of $(Cr,Al)_2O_3$. $Ni(Cr,Al)_2O_4$. NiO. Particularly, $Ni(Cr,Al)_2O_4$ and NiO particles embedded in chromia could act as crack nuclei. Upon the volumetric change induced by the oxidation, cracks propagate into the ceramic and grow in a cleavage mode, leading to the separation of TBC.

Due to failure method of these coatings, non-destructive evaluation of failure at inner layers of these coatings is important. By means of impedance spectroscopy method, changes of resistance and capacitance associated with degradation, oxidation and crack growth can be measured. Different researchers showed impedance spectra are sensitive to the thickness of different layers in TBCs. J. Mei *et.al* showed with increasing the oxidation time from 200 to 400 hours in Yttrium Stabilized Zirconia TBCs, impedance spectra shows two and three relaxation processes respectively. This suggests

that 200 hours oxidation time is not enough to make a continuous mixed oxide layer but with 400 hours oxidation time, they obtained three distinct layered: top-coat layer, alumina layer and mixed oxide layer.

In this study impedance spectra of ceramic APS spinel ($MgAl_2O_4$) and HVOF alumina coatings in varying frequency was studied to understand dielectric behavior and polarization features of these coatings. Following that, defect growth in air plasma spinel coatings subjected to cyclic micro-strain by means of electrical characterization has been studied.

2.3. $MgAl_2O_4$ (Spinel) ceramic coating

Spinel is a ternary oxide with general formula of AB_2O_4. A represents divalent cation and usually occupies a tetrahedral site and B represents trivalent metal cation in octahedral sites of cubic packed crystal [37]. Spinel is a ceramic material that due to its good mechanical, chemical, thermal and optical properties has wide range of applications in metallurgical, chemical, optical, catalysis and electronic industries such as refractory ceramics, electrical dielectric materials, and irradiation resistant materials. It has been used also as a humidity sensor, and ultrafiltration membrane [38, 39]. Various techniques have been applied to produce magnesium aluminate spinel such as Sol-gel, plasma spray, HVOF and hydrothermal technique.

2.4. Sample preparation

Spinel and alumina ceramic coatings were deposited on aluminum cantilever samples by air plasma spray and high velocity oxy-fuel method respectively. Thickness of the spinel coatings is between 180 to 330 microns and for alumina coatings is between 95 to 100 microns. Aluminum substrate

is treated as a conductive material without effect on results of electrical measurements. Aluminum surface (substrate) was polished to obtain smooth surface before doing electrical measurements to eliminate ceramic particles on the bottom side to have a good contact with bottom electrode of dielectric fixture.

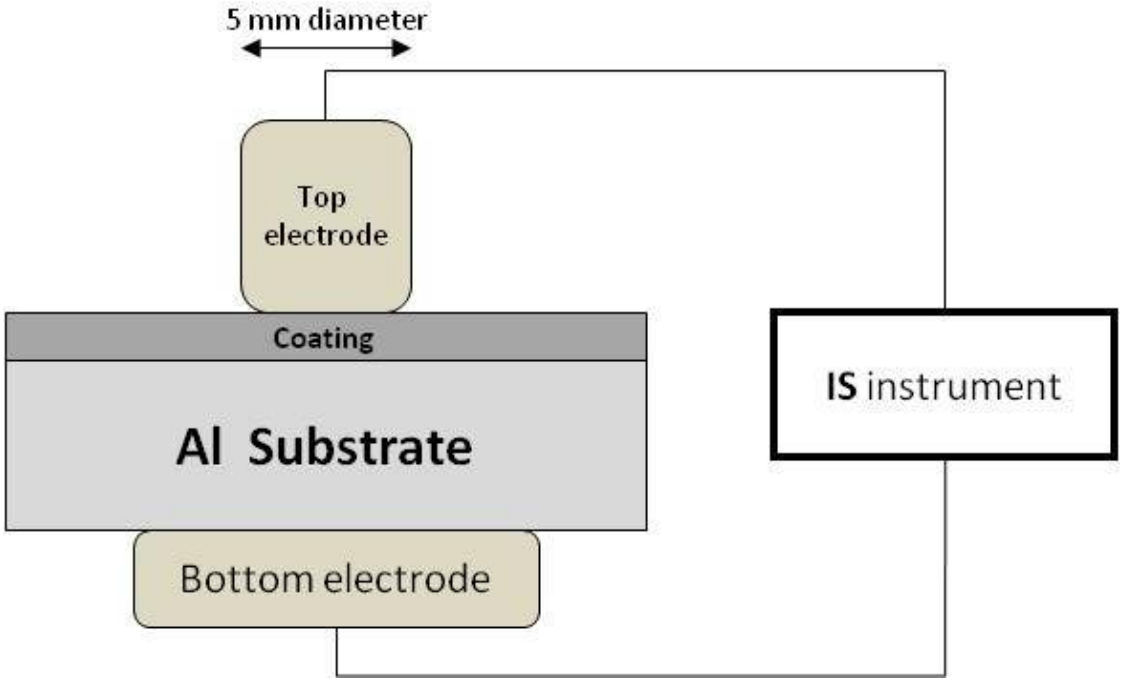

Figure 10. Schematic of electrical measurement setting

2.5. Measurements: capacitance and dissipation factor

2.5.1. Capacitance measurement

Dielectric properties of coatings were measured using impedance analyzer, Hewlett Packard HP4192A with parallel plate dielectric fixture. Figure11 is schematic of electrical measurement setting with parallel plate dielectric fixture. The specification of instrument is summarized in Table 1. Figure.11 shows the typical accuracy of the impedance analyzer. The overall dielectric behavior of ceramic spinel is explained by Maxwell-Wagner interfacial polarization theory. This explanation is in a good agreement with Koop's theory [41]. Maxwell-Wagner theory considers spinel material made of conducting grains with poor conducting grain boundaries. Figure12 shows capacitance versus frequency for this coating. This graph shows broader interfacial polarization features in comparison with Figure8. This can be due to polycrystalline and layered porous structure of thermally sprayed coatings, especially air plasma sprayed. These coatings exhibit more interfaces in different orientations. In such systems, different conduction mechanisms for the accumulation of charges at interfaces are responsible to obtain broader interfacial polarization features. Presence of this peak is due to strong correlation between conduction mechanism and dielectric behavior in spinel where frequency of electron vibration may be matching with the applied external field and it gives maximum loss [42].

Figure 13 shows capacitance spectra in various frequencies for HVOF alumina coating and bulk alumina. For HVOF alumina coating broad interfacial polarization is distinguishable, but bulk alumina exhibits very narrow interfacial polarization features. With increasing frequency capacitance is affected by frequency.

Table.1 accuracy of HP 4192A impedance analyzer.

Frequency ranges	**DC bias**	**Oscillation level**	**Impedance ranges**	**Capacitance ranges**
5 Hz ~ 13 MHz	± 35 V	5 mV ~ 1.1 Vrms	1 Ω ~ 1 MΩ	0.1 fF ~ 100 mF

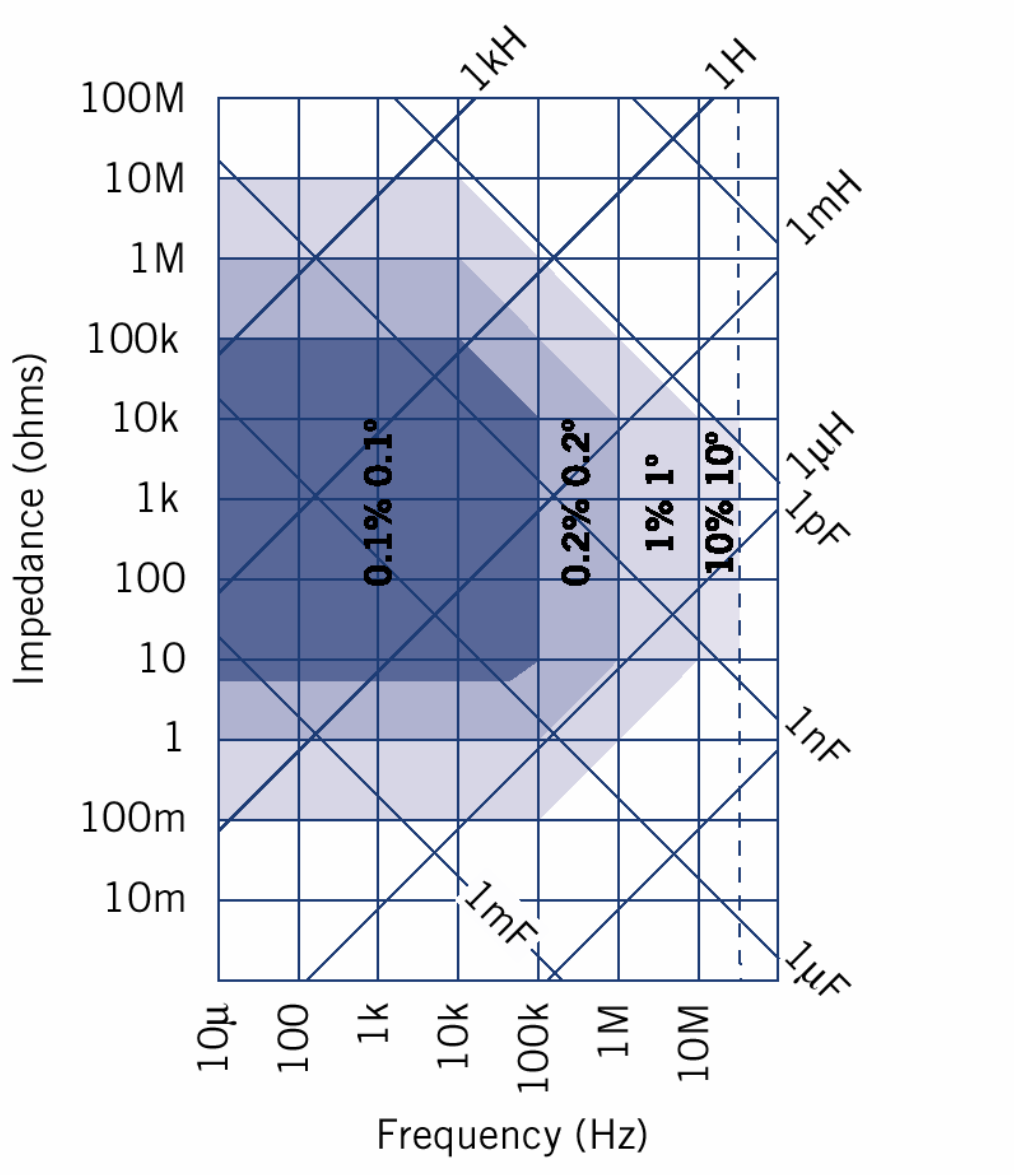

Figure 11 (a) Window of operation for Solartron1260 and for HP 4192A (thick solid line, <1% error). From the manual.

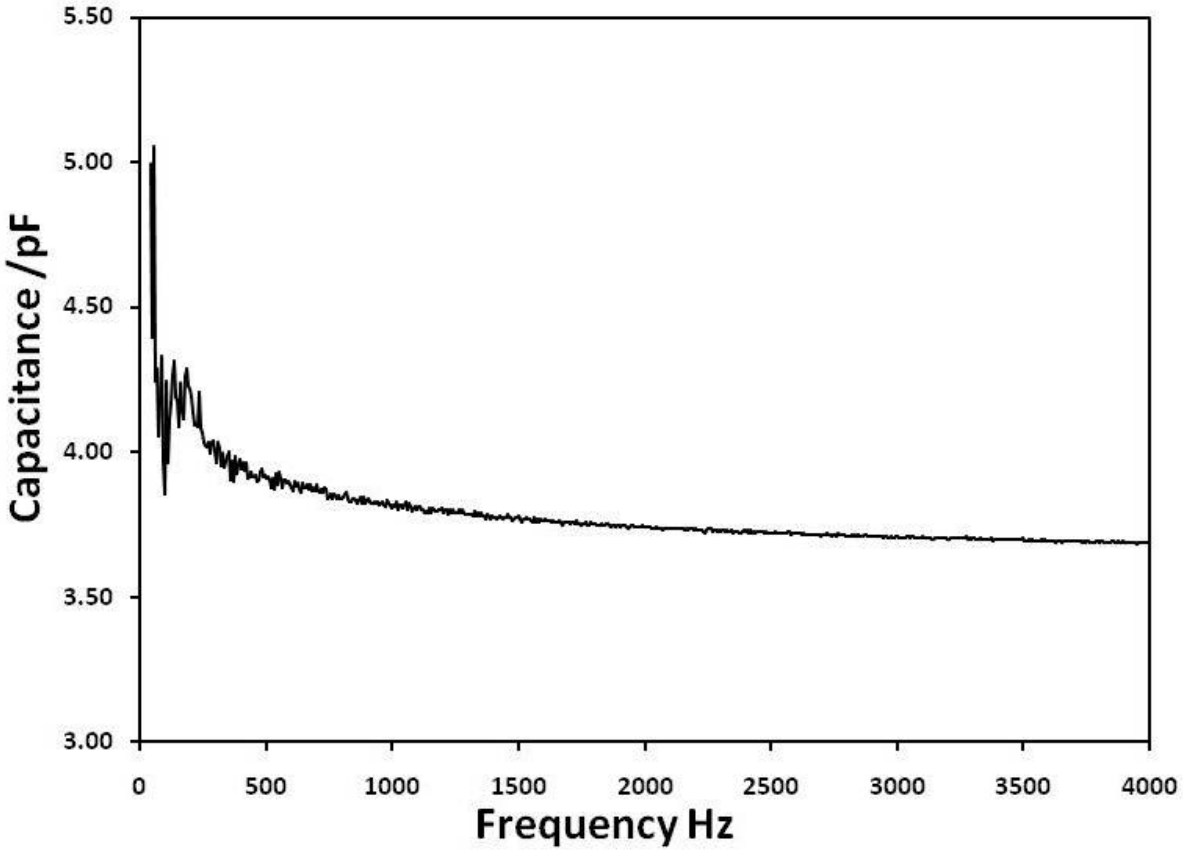

Figure 12. Broad interfacial polarization features in air plasma sprayed $MgAl_2O_4$

2.5.2. Dissipation factor

The ratio of the power loss in a dielectric material to the total power transmitted through the dielectric, the imperfection of the dielectric. Equal to the tangent of the loss angle (dimensionless):[40]

Equation 13 $$D = \frac{\varepsilon''}{\varepsilon'} = \tan\delta = \frac{1}{2\pi f C_p R_p}$$

Where

f = applied frequency

C_P = equivalent parallel capacity

R_P = equivalent parallel resistance

δ = loss angle

Figure 14 shows the dissipation factor of Spinel coating in different frequency. It shows a sharp increase at lower frequencies and decreasing with increasing the frequency. The rate of energy storage by the field is determined by ω whereas the rate of energy transfer to molecular collisions is determined by 1/τ. When ω=1/τ, the two processes, energy storage by the field and energy transfer to random collisions, are then occurring at the same rate, and hence energy is being transferred to heat most efficiently. This process is known as dielectric resonance, which we see in lower frequencies in Figure 14 and Figure 15 for bulk alumina and HVOF alumina coating.

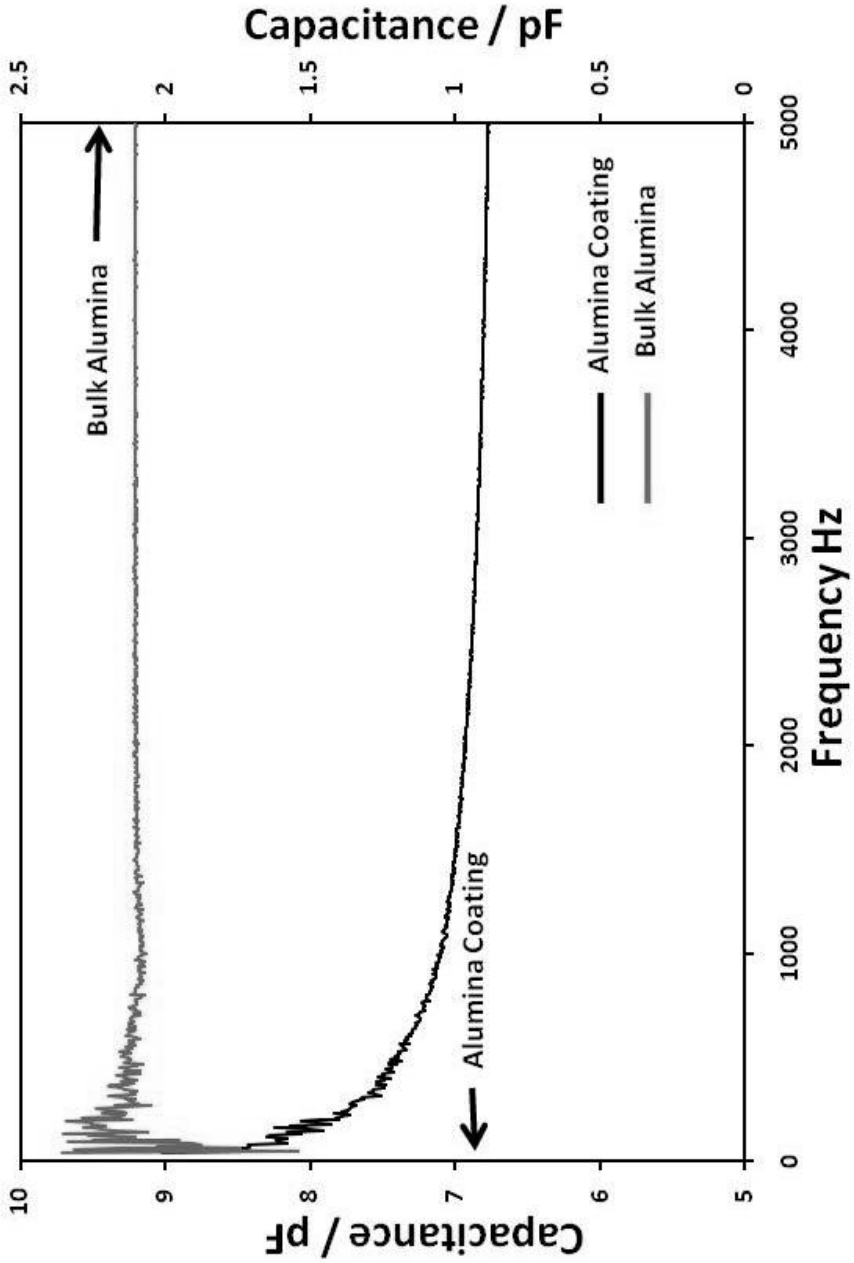

Figure13. capacitance of coating and bulk alumina Vs. frequency

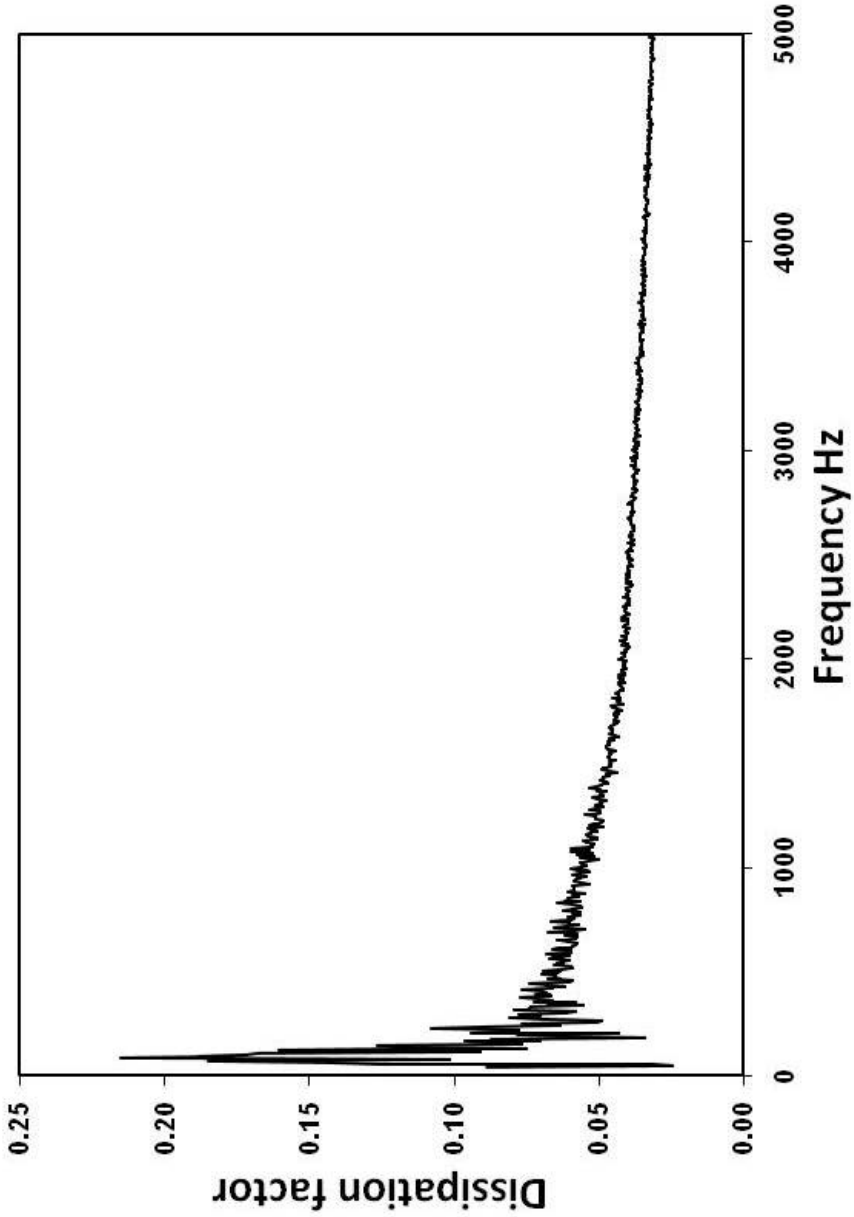

Figure 14 dissipation factor of spinel coating (same coating in Figure10)

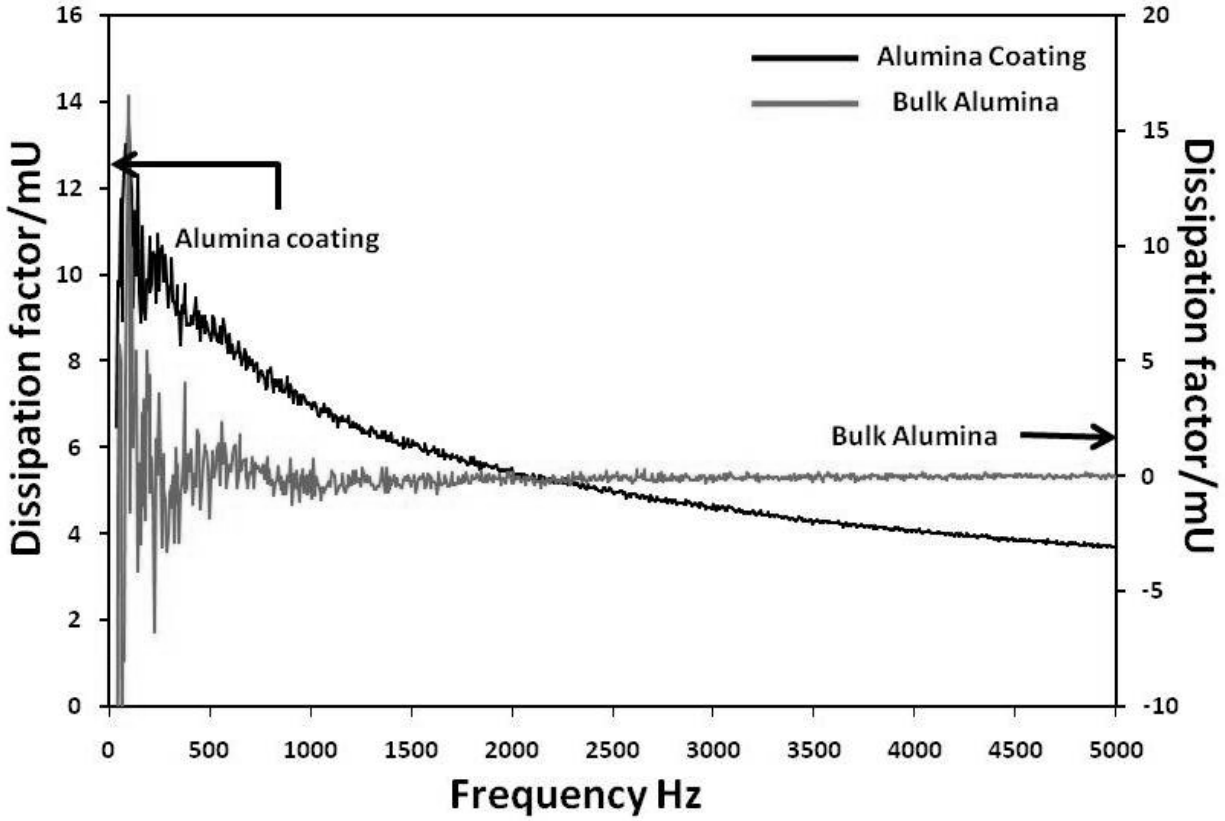

Figure 15 dissipation factor for HVOF alumina coating and bulk alumina in various frequency.

Chapter 3: Effect of humidity on electrical measurement of alumina and spinel

Ceramics have been studied for use in humidity sensors as a porous sintered body. $MgAl_2O_4$ has been investigated as a bulk form for humidity sensor. Also same authors have studied $MgAl_2O_4$ sensitivity to humidity in form of thin film. The results are in terms of resistance versus relative humidity and response time [43-46]. Conduction mechanism in both bulk and thin film $MgAl_2O_4$ has been considered as ionic. There is two stages for adsorption of water on the oxide surface:

I. Chemical adsorption of water on the surface with formation of hydroxyl ions. (So first layer of water)
II. With increasing humidity level, layers of water molecules are physisorbed on the hydroxyl layer and previous layer of water molecules. The physisorbed water easily dissociates to form H_3O^+ because of the high electrostatic fields in the chemisorbed layer.

De With *et.al* showed hydroxylation process takes place by adsorbing dissociated water molecules onto surface cation-oxygen pairs in such as way that the $(OH)^-$ is bonded to a surface cation and the H^+ to a surface oxygen atom. The calculations showed that hydration is favored on all the surfaces.

More than one monolayer physisorbed water on the surface, leads to higher carrier concentration. These hydrogen-bonded molecules are able to form dipoles and to reorient freely under an externally applied electric field, and form a liquid-like network, which increases the dielectric constant and, therefore, the proton concentration [47].

Physisorption of water molecules takes place at temperatures lower than 100˚C. At higher temperatures chemisorption of water molecules is responsible for electrical conductivity of spinel. Surface hydroxyls start to desorb at about 400˚C [48,49]. For studying the water adsorption in a structure, in addition to surface interaction with water molecules, the interaction between the porous structure and water must be considered. The amount of adsorbed water in pores depends on pores size and their distribution. There is a critical pore size that water adsorption happens in the pore with greater radius than critical radius. The following equation relates the critical pore size to temperature and water-vapor pressure.

Equation 14 $$r_k = \frac{2\gamma M}{\rho RT \ln(P_s/P)}$$

r_k is the Kelvin radius, P is the water vapor pressure, P_s is the water vapor pressure at saturation, and γ, ρ, and M are the surface tension, density and molecular weight of water, respectively. The smaller the r_k, or the lower the temperature, the more easily condensation occurs.

For our case with considering P/P_s = 40%, surface tension of water 0.07198 J/m^2 at room temperature, Kelvin radius will be 1.144×10^{-6} m.

For understanding the kinetics of water adsorption in spinel and alumina coatings in terms of capacitance, capacitance measurement was conducted for APS spinel coating and HVOF Alumina coating in differing partial pressure of water as a driving force versus exposure time. The experiment procedure was as follow: as-sprayed APS spinel and HVOF alumina coatings exposed respectively to atmosphere with 13.3 hPa and 8.55 hPa water partial pressure

for long time to get saturated. After that, coatings exposed to the atmosphere with 28.2 hPa (spinel) and 26.92 hPa (Alumina) water partial pressure and with starting exposure, capacitance measurement was started with 10 seconds steps between each measurement. Figure 16, Figure 17. The results show increasing in capacitance with exposing the samples to higher water partial pressure (ΔP=15 hPa for spinel and ΔP=18.42 for alumina) and decreasing the capacitance with decreasing the partial pressure of water. This behavior is due to increasing of thickness of water layer in the adsorption stage in pores within the coating and on the surface of coating as well. This observation is in agreement with multimolecular adsorption theory (BET isotherm) [50]. In desorption stage, as we see, the end point doesn't show same capacitance value as starting point which indicates the number of adsorbed molecules and desorbed molecules are not same. To desorb all adsorbed molecules, de-bonding of bonded molecules, we need more energy than bonding energy. Adsorption and desorption stages in two cases show two distinct convex and concave regions. However, these two regions are remarkable in desorption stage. It has been attributed to evaporation in the capillaries of the adsorbent in much lower temperature that of water evaporation temperature. Also it can be due to de-formation of multimolecular layers of adsorbed water.

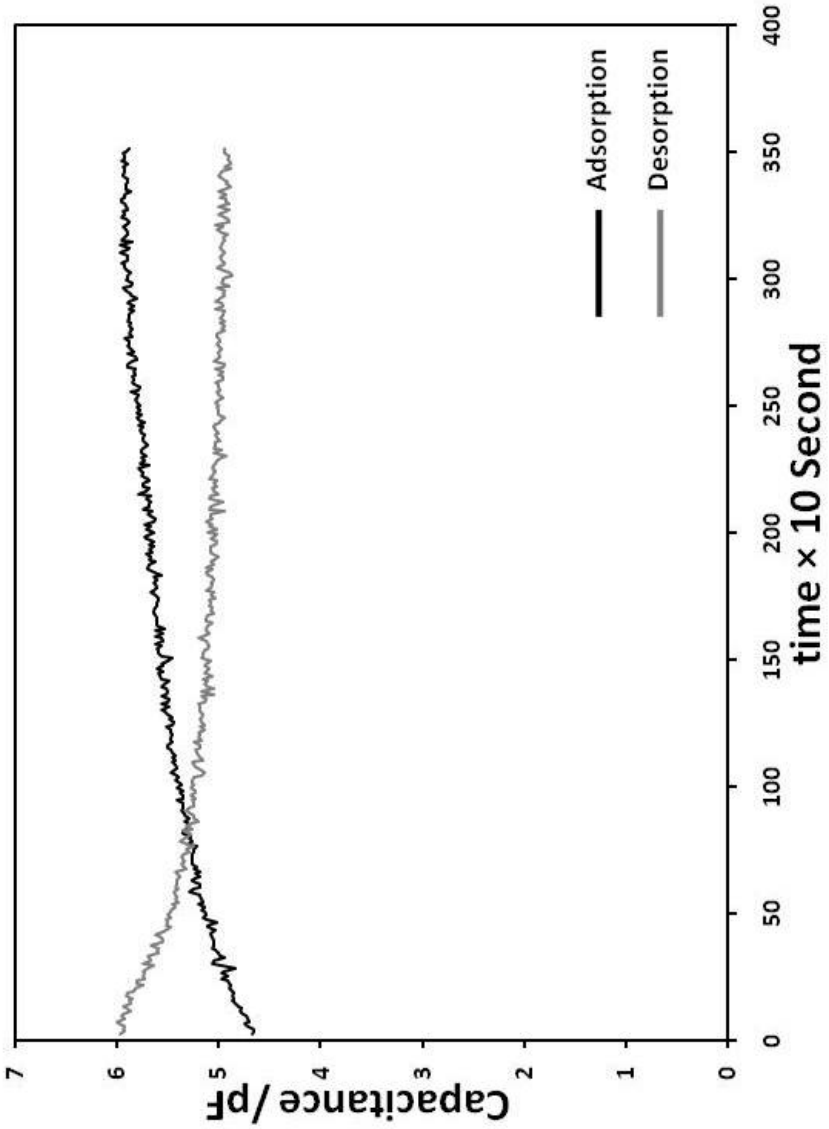

Figure 16 kinetics of adsorption and desorption of water in terms of capacitance for APS spinel coating

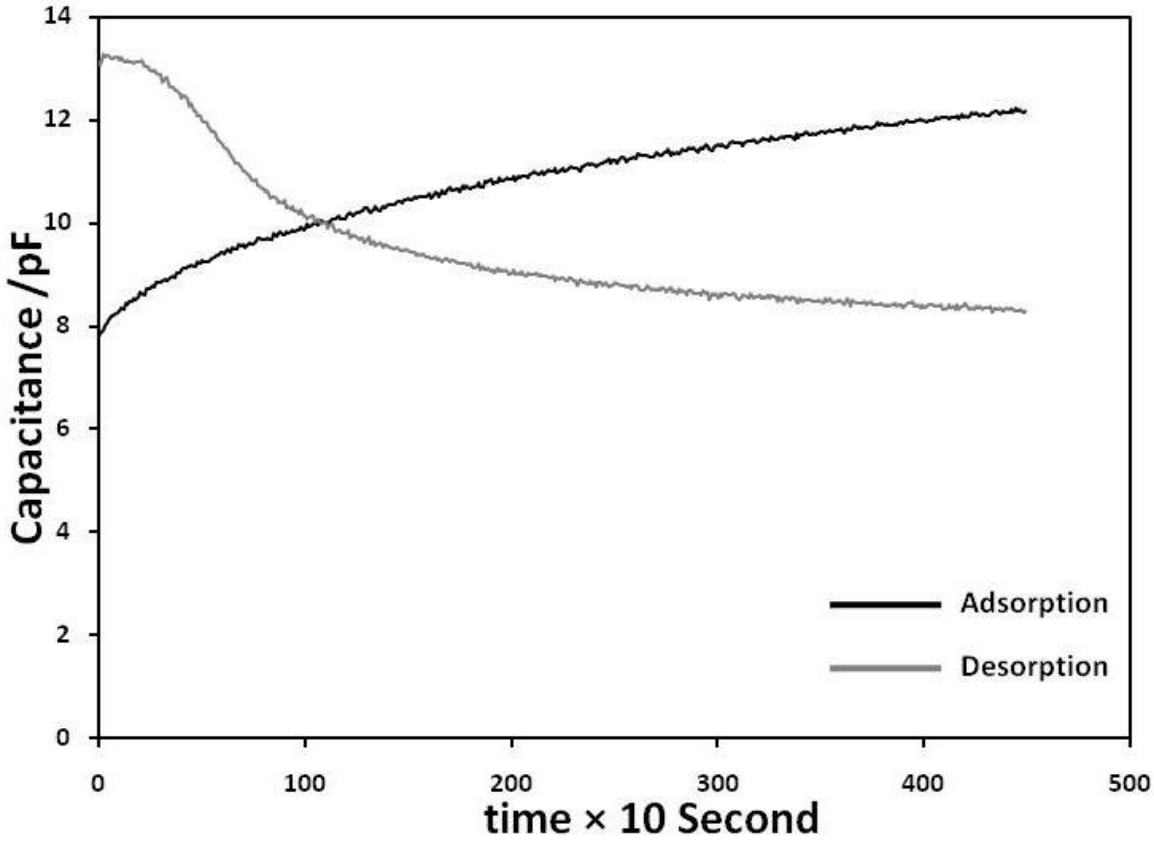

Figure 17 kinetics of adsorption and desorption of water in terms of capacitance for HVOF Alumina coating

3.1. Capacitance measurement of Spinel coating samples

Capacitance of six spinel samples was measured and based on thickness of each coating dielectric constant was calculated. Table.2 shows the capacitance, thickness and dielectric constant of each sample. Capacitance measurement was conducted at 2 KHz at same relative humidity for all six samples. Dielectric constant results show fluctuating from 6 to 10 for spinel samples, we hypothesize this difference is due to difference in thickness of the gap in between two splats.

3.1.1. Model for dielectric constant for spinel samples

To calculate the gap between two splats from measured capacitance, a series capacitance model was developed. In this model, each coating contains of three different materials that are considered as three capacitances in series:

I. ***Splats:*** Each splat was treated as a single crystal spinel with dielectric constant of 8.5. Thickness of each splat is calculated based on flattening ration of 4.

II. ***Air gaps:*** between two splats there is an air gap with unknown thickness that is calculated as result of modeling. Dielectric constant of air gap is considered 1.

III. ***Water layer:*** thickness of water layer in each air gap is considered 150 nanometers. Dielectric constant of water layer is considered 80.

With this model after measuring the thickness of coating we are able to calculate number of splat layers present in the coating.

Table.2 Dielectric constant,capacitance and thickness of air gap between two splats

Samples	*CS-160*	*CS-159*	*CS-158*	*CS-155*	*CS-154*	*CS-153*
Capacitance(pF)	7.09	6.34	5.41	6.68	5.42	6.11
Thickness of coating(mm)	0.25	0.2	0.22	0.24	0.33	0.211
Dielectric constant	10.20	7.30	6.85	9.23	10.29	7.42
Volume of water/Volume of air gap × 100	97.53%	82.69%	79.96%	93.05%	97.87%	83.47%
Thickness of air gap(nm)	153.8	181.4	187.6	161.2	153.2	180

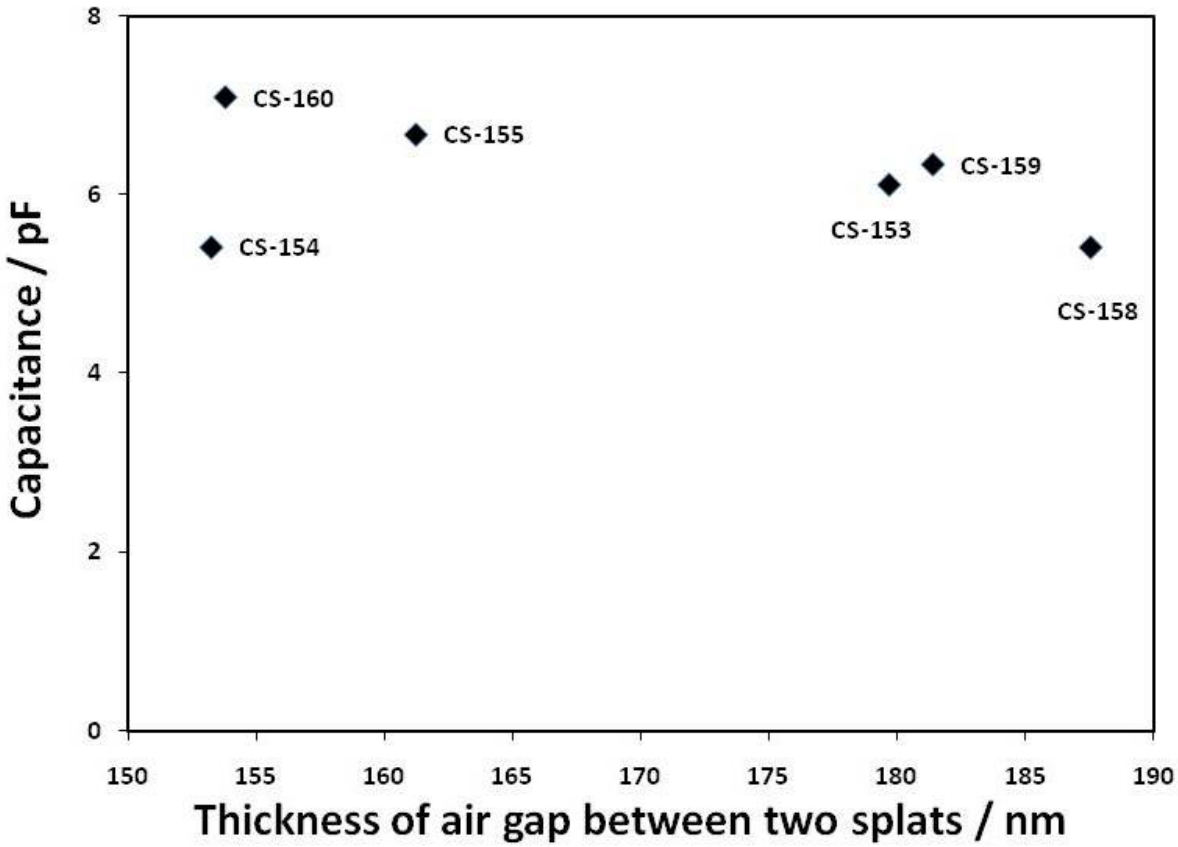

Figure18 Measured capacitance for each sample versus calculated air gap thickness between two splats

With known number of total layers, thickness of water layer, thickness of each splat we can obtain thickness of air gap between two splats. Figure 18 shows measured capacitance of each sample versus thickness of air gap that doesn't show particular relation but if we draw same graph for measured dielectric constant,, with increasing thickness of air gap from 153 to 187 nanometers dielectric constant will decrease 10.3 to 6.85. Figure 19.

3.2. Surface hydroxylation of spinel coating

To study the hydroxylation of spinel coating by electrical measurement, capacitance of coating was measured before and after baking at 220°C for 30 minutes. Figure 20 shows increasing of capacitance with increasing the time of exposure to the humid air, but value for capacitance doesn't reach to capacitance value before baking. We hypothesize two reasons for this observation:

I. Changing the surface chemistry due to hydroxylation which reduces the available sites for water molecules. This reaction can take place as follow:

   $MgAl_2O_4 + 4H_2O \rightarrow Mg(OH)_2 + 2Al(OH)_3$

II. Due to baking, pores and cracks within the coating get closed and in this way there is less surface area for adsorbing water molecules into the structure.

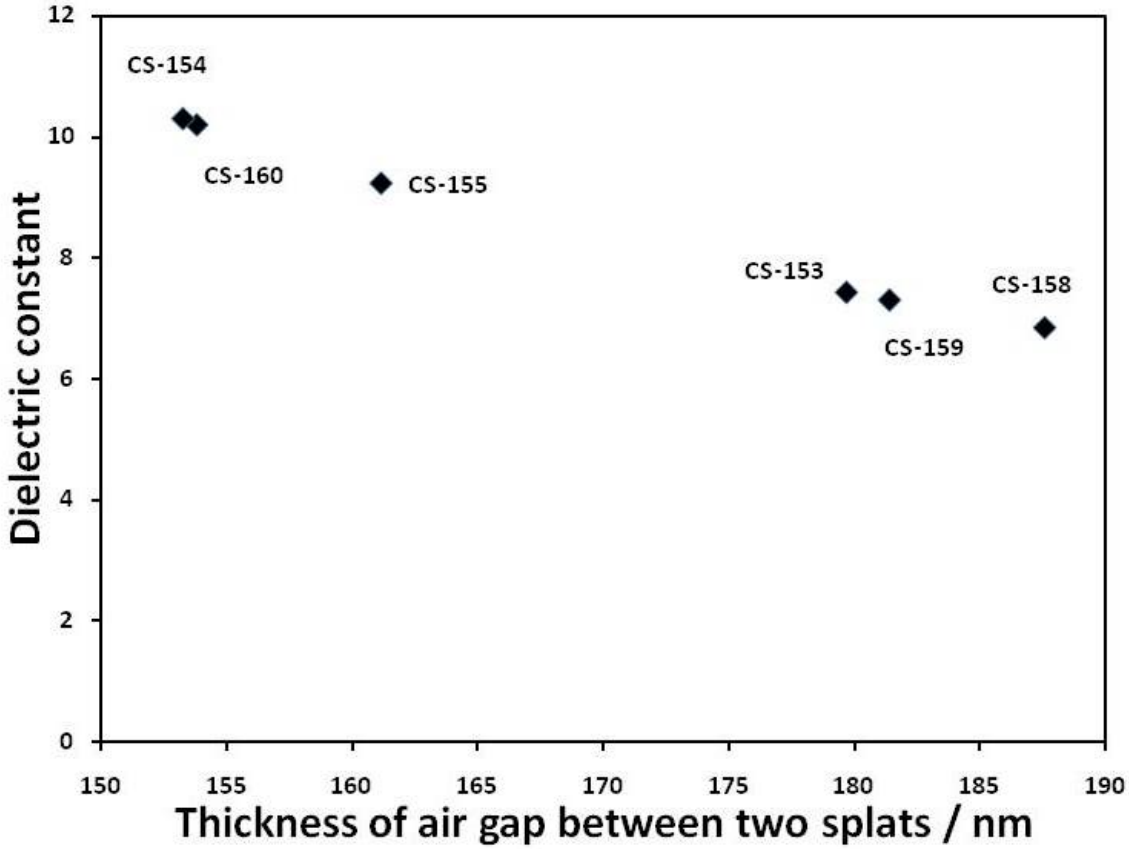

Figure 19 Measured dielectric constant for each sample versus calculated air gap thickness between two splats

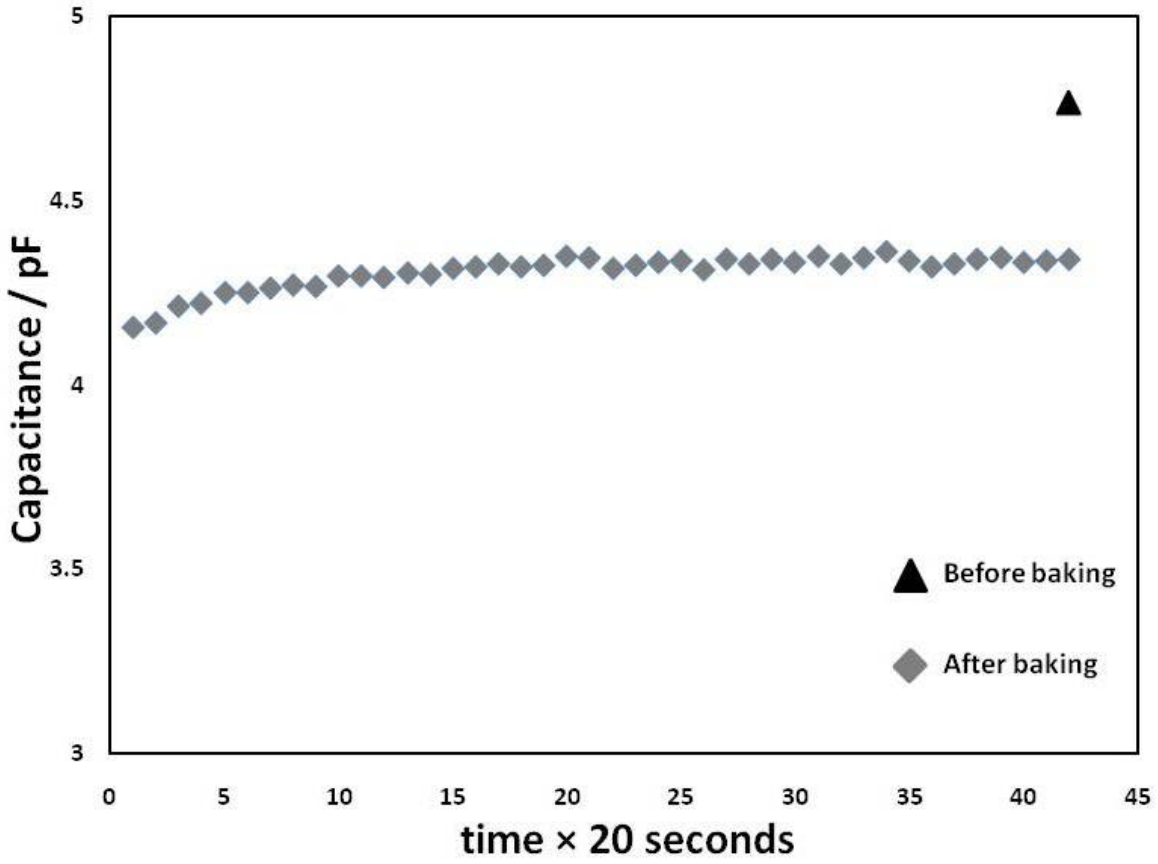

Figure 20 Capacitance of spinel coating before and after baking.

Chapter 4: Electrical characterization of defect evaluation in thermally sprayed ceramic coatings subjected to cyclic micro-strain

The focus of this research is to understand the microstructural changes that occur under low strain cycling of air plasma sprayed (APS) coatings. Preliminary data shows that under nominally elastic loading (<< 0.1% strain) of thermally sprayed materials changes occur that are detectable via electrical (resistivity, dielectric constant) measurement methods. This is due to the micro-scale growth of pre-existing defects; our study is unique as most other 'fatigue' tests on thermally sprayed materials are suited for cycles to failure, etc. To systematically test this, we deposited spinel coatings on tapered cantilever Aluminum substrates, which were flexed to provide spatially constant in-plane cyclic strains. After different numbers of cycles, dielectric constant of coatings was measured via impedance spectroscopy. Results confirm growth of defects under these low strains, and also a large effect of humidity on different porosity features. We explain this by recourse to physisorption and chemisorptions of water molecules on crack faces. Physisorption and chemisorption phenomena have been discussed in previous chapter more in detail. Our investigation could have major implications for coating reliability, as it allows us to characterize how a coating evolves in-service.

Air plasma sprayed spinel coatings with thickness range 180 to 330 micron were made. Spinel ($MgAl_2O_4$) powder (5-20 micron) was used. Coatings were deposited on Aluminum tapered ('strain along the center line is constant') cantilever substrates Figure21a. To apply cyclic strain to coatings, we used a

fatigue test machine designed for cantilever samples with an eccentric shaft to apply different bending amplitudes Figure 21b. Here we applied tension and compression. To calculate the strain ε to which the coating is subjected, we treat it as a thin film on a thick substrate of thickness t, giving us the following equation.

Equation 14 $\varepsilon = (At/L^2)$

Here (A) is applied amplitude and (L) is the length of the sample and (t) is the thickness of coating and substrate together.

Before and after different stages of cycling, coating dielectric constant was measured via impedance spectroscopy, at 2 kHz. At 2 kHz frequency we are able to pick up interfacial effects of dielectric which might increase due to cycling of coating. Ten measurements were taken along the sample length, for sampling average. The radius of electrode was large enough in comparison with volume and length of present defects (5 mm in diameter). In addition, to test the effects of humidity, some samples were baked at 210°C for 30 minutes, and dielectric constant was measured as a function of time (20 seconds increments) exposed to room (humid) air. Maximum applied strain for the thickest sample was 4.8×10^{-4}.

Figure 22 shows capacitance of unbaked spinel samples, as a function of increased number of strain cycles. Capacitance increases and then stabilizes after a few thousand cycles. This suggests more water molecules adsorption in the coating which is due to a strain-controlled fatigue mechanism in the coatings – that is to say, as the coating is cycled, cracks grow, increasing local compliance and reducing local stress intensity factor, in turn slowing growth. However, if one considers that cracks contain air (dielectric constant = 1), one

would expect a decrease in capacitance with crack growth. This discrepancy can be explained by considering the adsorption of water on crack surfaces; water has a higher dielectric constant (78.4) than spinel (10).

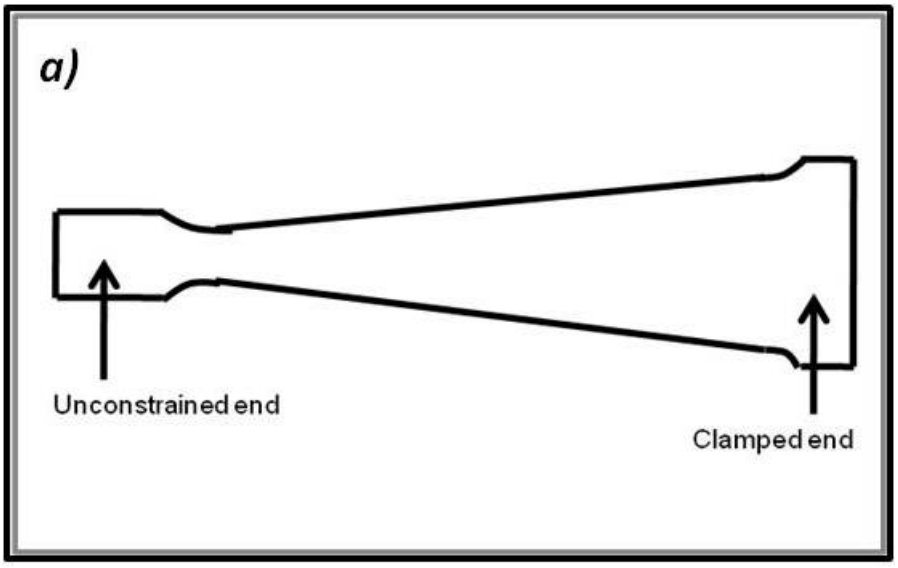

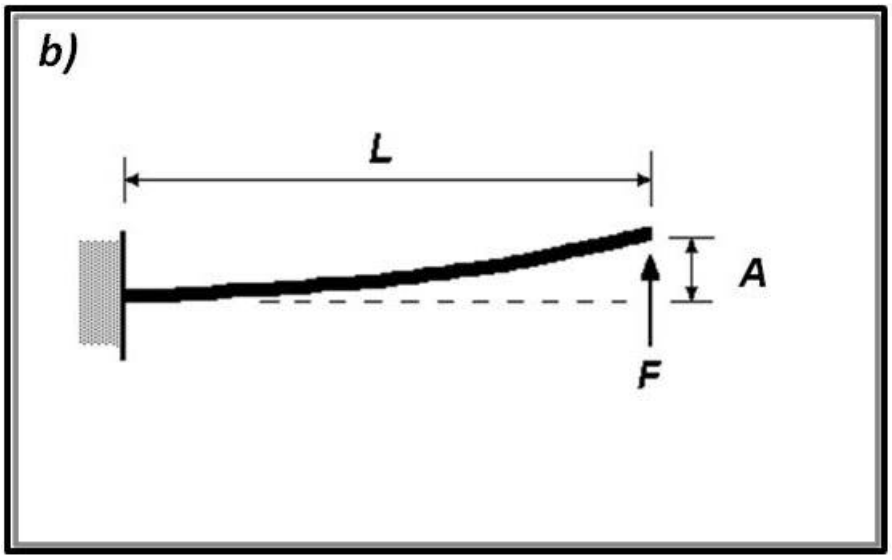

Figure 21 a) schematic of tapered cantilever sample, b) schematic of applied amplitude to unconstrained end of cantilever sample.

The baking out experiments was done to isolate such humidity effects. Figure 23 shows capacitance versus time for baked samples exposed to humid air, after different cycling stages (as-sprayed, 1000, 2000, 5000, 10000). In all cases, capacitance increases with time, indicating water adsorption. As explained in previous stage However, with cycling, overall capacitance decreases. This suggests:

I. The existence and growth of "closed" cracks in the coating that tend to decrease dielectric constant, made possible by,
II. Irreversible reactions in such closed cracks, during bake out. In other words, after baking, water vapor may enter open cracks, increasing capacitance with time, but not closed cracks. This data suggests a way to distinguish between open and closed cracks in ceramic coatings, and also to understand specifically which defects grow under applied (nominally elastic) cyclic strains.

With this set of experiments we showed that defects in thermally sprayed ceramic coatings can grow in much lower strain (nominally elastic) than elastic strain. This crack growth associated with crack bridging mechanism. This crack bridging is due to frictional wear of sliding ligaments when cracks open and close again and again under cyclic strain. In case of thermally sprayed coatings we can consider the coating contains of splats with interfaces in between them. The interfaces are not very well bonded together and have weak bonding points. With applying cyclic strain weak points break and connect two neighbor cracks and make one bigger crack instead of two

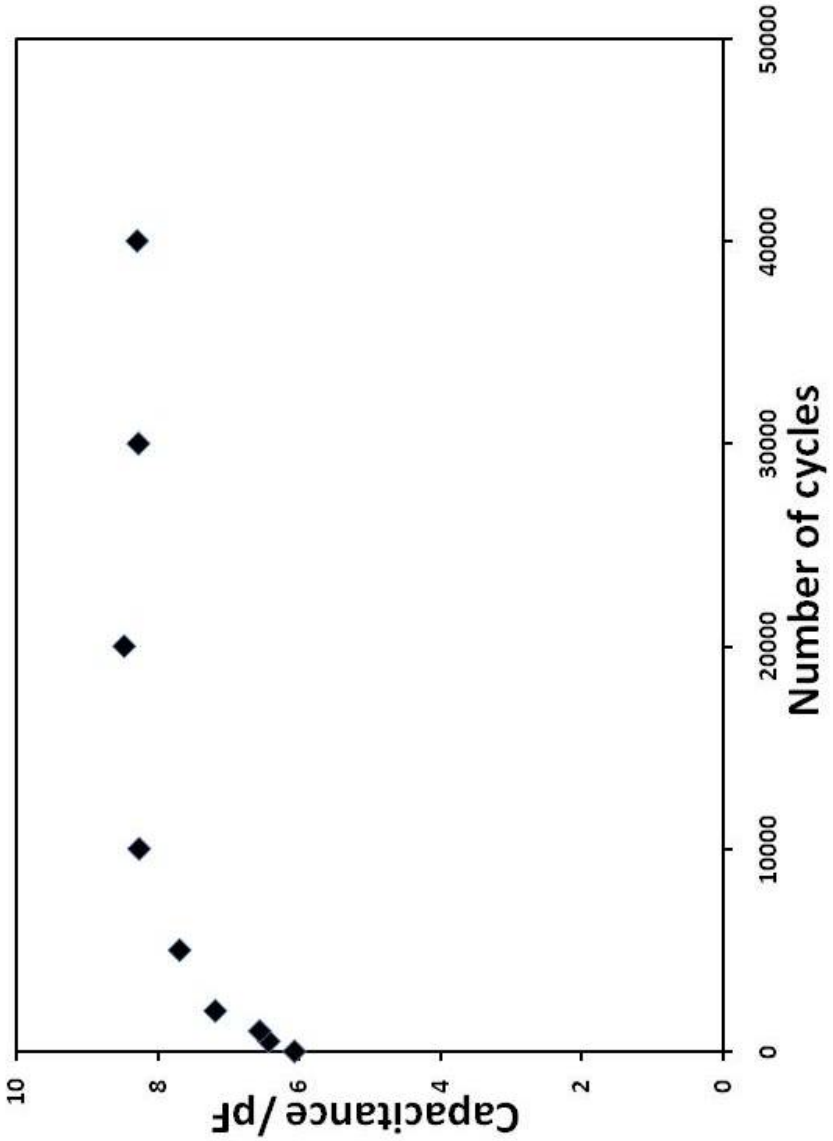

Figure 22 Capacitance versus number of applied cycles for unbaked spinel sample.

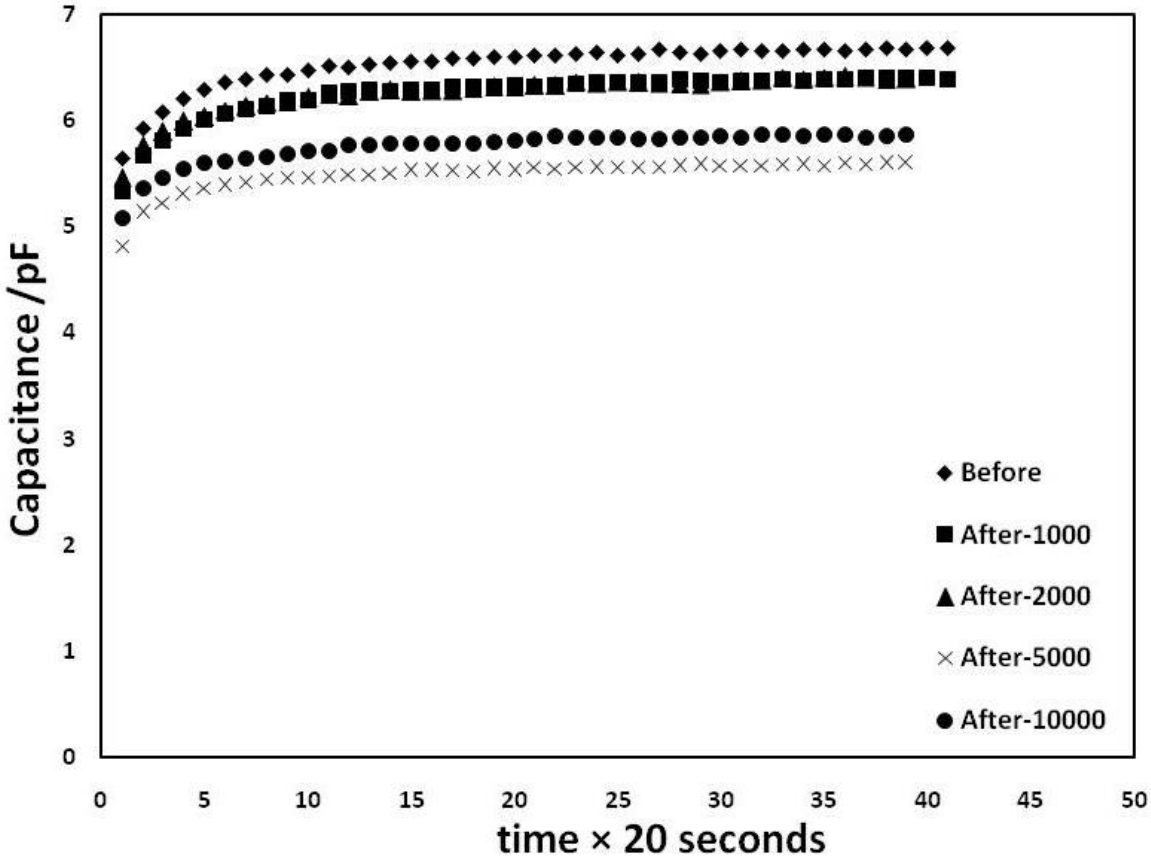

Figure 23 Capacitance versus number of applied cycles for unbaked spinel sample.

small cracks. Our data showed saturation of cracks under applied cyclic strain after thousands of cycles.

Chapter 5: References:

[1] S. Suresh. Fatigue of materials. 2nd edidtion. Cambridge: 1998.

[2] B. R. Lawn, T. R. Wilshaw. Fracture of brittle solids. Cambridge:CUP, 1975.

[3] M. Li, F. Guiu. Subcritical fatigue crack growth in alumina. Acta metal. Mater. 1995;43:1871.

[4] Y.-H. Huh, J.-H. Song. Cyclic fatigue crack growth and closure behavior in alumina ceramics. Fatigue and fracture of engineering materials and structures. 1998;21:1575

[5] R.O. Ritchie. Mechanisms of fatigue-crack propagation in ductile and brittle solids. International journal of fracture. 2004;100:55.

[6] R. H. Dauskardt,. A frictional-wear mechanism for fatigue-crack growth in grain bridging ceramics. Acta. Metal. Mater. 1993;41:2765.

[7] S. Lathabai, Y. W. Mai and B.R.Lawn,. Cyclic fatigue of an alumina ceramic with R-curve characteristic. J.Am.Ceram. Soc. 1989;72:760.

[8] S.Lathabai, J. Rodel and B.R. Lawn,. Fracture and deformation damage accumulation in tough ceramics. J. Am. Ceram. Soc. 1991;74:1340.

[9] F. Guiu, M. Li and M. J. Reece,. Role of crack-bridging ligaments in the cyclic fatigue behavior of alumina. J. Am. Ceram. Soc. 1992;75:2976.

[10] X. Z. Hu, and Y. W. Mai,. Crack bridging analysis for alumina ceramics under monotonic and cyclic loadings. J. Am. Ceram. Soc. 1992;75:848.

[11] M.E. Ebrahimi, J. Chevalier, and G. Fantozzi. Slow crack-growth behavior of alumina ceramics. J. Mat. Res. 1999.

[12] N. J. van der Laag, A. J. M. van Dijk, N. Lousberg, and G. de With. The influence of water on the fracture of magnesium aluminate (MgAl2O4) spinel. 2005.

[13] A. J. Mcevily and R.W. Staehle. Corrosion fatigue. Nat. Assoc. Corrosion eng. 1972, Houston

[14] G. E. Dieter,. Mechanical metallurgy. 3rd edition. McGrawHill:1986.

[15] A.R. Jones. Microcracks in hard chromium electro deposits. Plating surf. Finish. 1989;62.

[16] G. Dulpernell, F.A. Lowenheim, modern electroplating. 1968;80.

[17] H. Kuo, J. Lai, T. Lin, Int. Arch. Occup. Environ. Health. 1997;70.

[18] M.P. Nascimento, H.J.C. Voorwald, R.C. Souza, I.M. Miguel, W.L. Pigatin, Surf. Coat. Technol. 2001;138:113.

[19] M.P. Nascimento, R.C. Souza, W.L. Pigatin, H.J.C Voorwald, Int. J. Fatigue. 2001;23.

[20] E.R. De los Rios, A. Walley, M.T. Milan, G. Hmmersley, Int. J. Fatigue. 1995;493:17.

[21] C.P. Diepart, Mat. Sci. Forum. 1994;457:163-165.

[22] M.A.S. Torres, H.J.C. Voorwald, Int. J. Fatigue. 2002;24:877.

[23] A.G. Evans, J. W. Hutchinson. Progress in materials science. 2001;46:249-71.

[24] A.G.Evans, D.R. Mumm, J.W. Htchinson, G.H. Meier, F.S. Pettit. Mechanisms controlling the durability of thermal barrier coatings. progress in materials science. 2001

[25] A. Vadiraj and M. Kamaraj. Characterization of fretting fatigue damage of PVD TiN coated biomedical titanium alloys. Surf. and Coatings Tech. 2006;200:4538

[26] H. Liang, B. Shi, A. Fairchild and T. Cale. Applications of plasma coatings in artificial joints: an overview. Vacuum. 2004;73:317. The 4th International Symposium on Applied Plasma Science

[27] Y. C. Yang and Edward Chang. Influence of residual stress on bonding strength and fracture of plasma-sprayed hydroxyapatite coatings on Ti–6Al–4V substrate. Biomaterials. 2001;22:1827

[28] A. Wan: I.M. Hutchings, Editor. New directions in tribology. World Tribology Congress, London. 1997:443–458.

[29] L. B. Freund and S. Suresh, Cambridge. thin film materials stress, defect formation and surface evolution.

[30] G. L. Hans, C. Terry, Chilcott and C. F. Adelle. Impedance spectroscopy of interfaces, membranes and ultrastructures. Bioelectrochemistry and Bioenergetics. 1996;40:79

[31] S.O. Kasap. Principles of electronic materials and devices. 3rd edition. Mcgraw-hill, 2006.

[37] E. H. Wallker Jr., J. W. Owens, M. Etinne and D. Walker, Mater. Res. Bull. 2002;37:1041-1050.

[38] R.C. Weast(Ed). handbook of chemistry and physics. 74th ed. CRC press, Boca Raton, FL, 1988

[39] W. Jones and L.J. Miles. Production of beta Al_2O_3 electrolyte. Proc. Br. Ceram. Soc. 1971;19:161

[40] http://composite.about.com/library/glossary/d/bldef-d1727.htm

[41] C. G. Koops. On the dispersion of resistivity and dielectric constant of some semiconductors at audiofrequencies. Physical Review. 1951;83:121.

[42] S. Angappan, L. J. Berchmans, C.O. Augustin. Sintering behavior of MgAl2O4 – a prospective anode material.

[43] T. Seiyama, N. Yamazoe, and H. Arai, Sens. Actuators. 1983;4:85.

[44] Y. Shimizu, H. Arai, and T. Siyama, Sens. Actuators. 1985;7:11.

[45] G. Gusmano, G. Monteperelli, P. Nunziante and E.Traversa, in ceramic transactions: ceramic powder science IV, edited by S.I. Hirano, G.L. Messing,

and H. Hausner,.The American Ceramic society, Westerville, OH,. 1991;22:545.

[46] G. Gusmano, G. Monteperelli, P. Nunziante and E.Traversa, Br. Ceram. Trans. 1993;92:104

[47] E. McCafferty and A.C. Zettlemoyer, Discuss. Faraday Soc. 1971;52:239.

[48] M. Egashira, S. Kawasumi, S. Kagawa and T. Seiyama,. Temperature programmed desorption study of water adsorbed on metal oxides: I., Bull. Chem. Soc. Jpn. 1978;51:3144-3149.

[49] M. Egashira, M. Nakashima, S. Kawasumi and T.Seiyama. Temperature programmed desorption study of water adsorbed on metal oxides: Tin oxide surfaces, J. Phys. Chem. 1981;85:4125-4130.

[50] S. Brunauer, P. H. Emmet and E. Teller. Adsorption of gases in multimolecular layers. 1938

[51] A. G. Cockbain and P. J. Harrop. The temperature coefficient of capacitance. BRIT. J. APPL. PHYS. (J. PHYS. D), 1968;1.